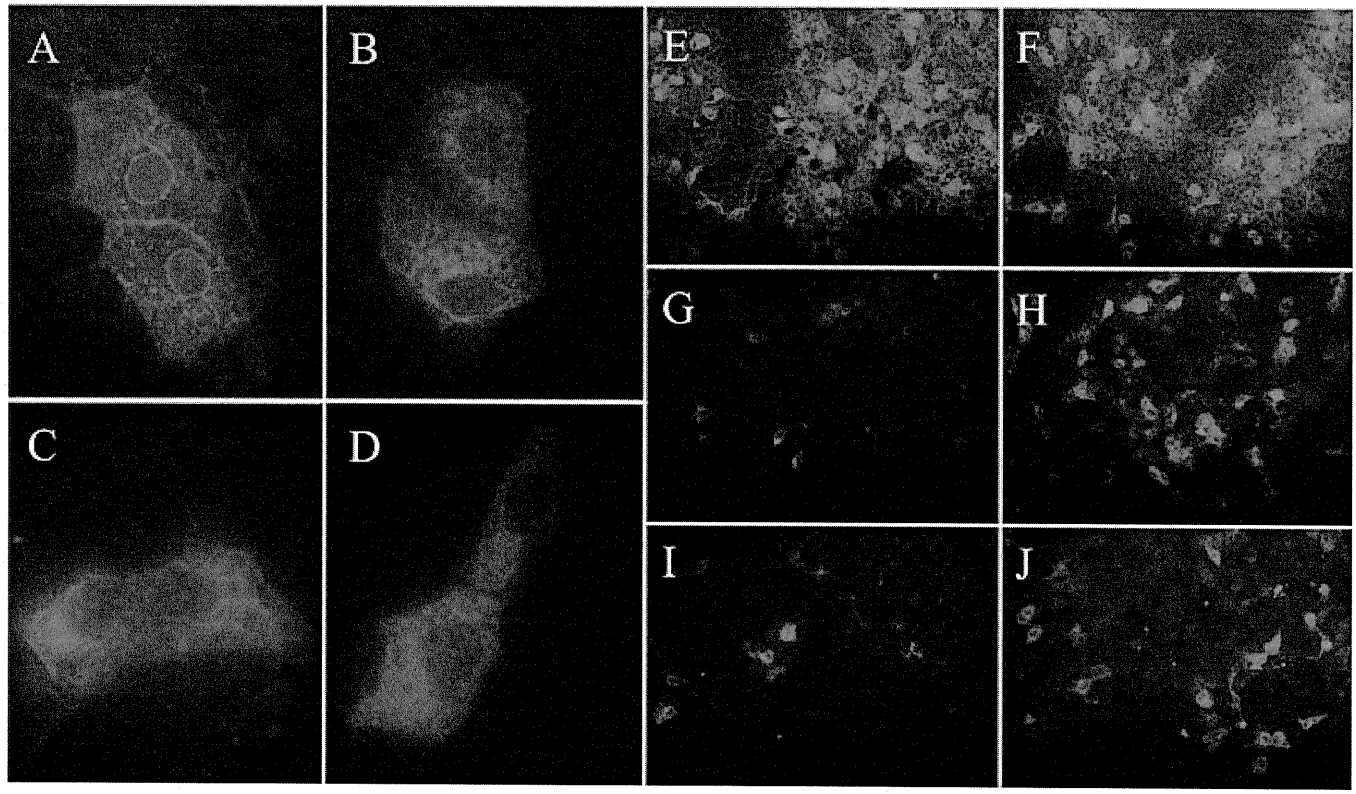

Figure 3. Results of the immunocytostaining analysis using anti-V5 antibody for the HCE-T cells transfected with expression vector harboring the wild-type or mutated TACSTD2 gene tagged with V5-epitope. Immunolocalization at the plasma membrane is apparent in the HCE-T cells transfected with the wild-type (**A**) *TACSTD2*. In HCE-T cells transfected with the mutated (**B**: p.Ile281SerfsX23, **C**: p.Tyr225X, **D**: p.Gln118X) *TACSTD2*, immunoreactivity was observed not at the plasma membrane but in the cytoplasm with slightly intensified signal around their nucleus. In the HCE-T cells transfected with wild-type *TACSTD2* (**E** and **F**), no apparent change was observed by the detergent treatment (0.1% Tween-20 for 30 min; **F**). However, in the HCE-T cells transfected with mutated *TACSTD2* (**G** and **H**: p.Ile281SerfsX23, **I** and **J**: p.Tyr225X), detergent treatment (**H**, **J**) significantly increased the number of the immunopositive cells as compared to those with no detergent treatment (**G** and **I**).

corneal epithelial cells in vitro. The TACSTD2 protein may have various unidentified functions other than those that we have already shown, and we hope that the findings presented in this study will provide the next step toward a better understanding of the pathogenesis of GDLD.

ACKNOWLEDGMENTS

We thank John Bush for reviewing the manuscript. This work was supported by a grant-in-aid (#21592238) from the Japanese Ministry of Education, Science, Culture and Sports and by a grant (H22-Nanchi-Ippan-057) from Japanese Ministry of Health, Labour and Welfare. This work was also supported by a research fund from the Kyoto Foundation for the Promotion of Medical Science.

REFERENCES

1. Nakaizumi G. A rare case of corneal dystrophy. Acta Soc Ophthalmol Jpn. 1914; 18:949-50.
2. FukjikiKKanaiANakajimaA.Gelatinous drop-like corneal dystrophy in Japanese population. (Abstract). 7th Int. Cong. Hum. Genet1986248–9
3. Kawano H, Fujiki K, Kanai A, Nakajima A. Prevalence of gelatinous drop-like corneal dystrophy in Japan. Atarashii Ganka. 1992; 9:1879-82.
4. Weber FL, Babel J. Gelatinous drop-like dystrophy. A form of primary corneal amyloidosis. Arch Ophthalmol 1980; 98:144-8. [PMID: 6986141]
5. Mondino BJ, Rabb MF, Sugar J, Sundar Raj CV, Brown SI. Primary familial amyloidosis of the cornea. Am J Ophthalmol 1981; 92:732-6. [PMID: 7030080]
6. Tsujikawa M, Kurahashi H, Tanaka T, Nishida K, Shimomura Y, Tano Y, Nakamura Y. Identification of the gene responsible for gelatinous drop-like corneal dystrophy. Nat Genet 1999; 21:420-3. [PMID: 10192395]
7. Ha NT, Chau HM. Cung le X, Thanh TK, Fujiki K, Murakami A, Kanai A. A novel mutation of M1S1 gene found in a Vietnamese patient with gelatinous droplike corneal dystrophy. Am J Ophthalmol 2003; 135:390-3. [PMID: 12614764]
8. Tasa G, Kals J, Muru K, Juronen E, Piirsoo A, Veromann S, Janes S, Mikelsaar AV, Lang A. A novel mutation in the M1S1 gene responsible for gelatinous droplike corneal dystrophy. Invest Ophthalmol Vis Sci 2001; 42:2762-4. [PMID: 11687514]

9. Ren Z, Lin PY, Klintworth GK, Iwata F, Munier FL, Schorderet DF, El Matri L, Theendakara V, Basti S, Reddy M, Hejtmancik JF. Allelic and locus heterogeneity in autosomal recessive gelatinous drop-like corneal dystrophy. Hum Genet 2002; 110:568-77. [PMID: 12107443]
10. Tian X, Fujiki K, Li Q, Murakami A, Xie P, Kanai A, Wang W, Liu Z. Compound heterozygous mutations of M1S1 gene in gelatinous droplike corneal dystrophy. Am J Ophthalmol 2004; 137:567-9. [PMID: 15013888]
11. Markoff A, Bogdanova N, Uhlig CE, Groppe M, Horst J, Kennerknecht I. A novel TACSTD2 gene mutation in a Turkish family with a gelatinous drop-like corneal dystrophy. Mol Vis 2006; 12:1473-6. [PMID: 17167402]
12. Murakami A, Kimura S, Fujiki K, Fujimaki T, Kanai A. Mutations in the membrane component, chromosome 1, surface marker 1 (M1S1) gene in gelatinous drop-like corneal dystrophy. Jpn J Ophthalmol 2004; 48:317-20. [PMID: 15295654]
13. Taniguchi Y, Tsujikawa M, Hibino S, Tsujikawa K, Tanaka T, Kiridoushi A, Tano Y. A novel missense mutation in a Japanese patient with gelatinous droplike corneal dystrophy. Am J Ophthalmol 2005; 139:186-8. [PMID: 15652848]
14. Zhang B, Yao YF, Zhou P. Two novel mutations identified in two Chinese gelatinous drop-like corneal dystrophy families. Mol Vis 2007; 13:988-92. [PMID: 17653040]
15. Alavi A, Elahi E, Tehrani MH, Amoli FA, Javadi MA, Rafati N, Chiani M, Banihosseini SS, Bayat B, Kalhor R, Amini SS. Four mutations (three novel, one founder) in TACSTD2 among Iranian GDLD patients. Invest Ophthalmol Vis Sci 2007; 48:4490-7. [PMID: 17898270]
16. Araki-Sasaki K, Ando Y, Nakamura M, Kitagawa K, Ikemizu S, Kawaji T, Yamashita T, Ueda M, Hirano K, Yamada M, Matsumoto K, Kinoshita S, Tanihara H. Lactoferrin Glu561Asp facilitates secondary amyloidosis in the cornea. Br J Ophthalmol 2005; 89:684-8. [PMID: 15923502]
17. Ide T, Nishida K, Maeda N, Tsujikawa M, Yamamoto S, Watanabe H, Tano Y. A spectrum of clinical manifestations of gelatinous drop-like corneal dystrophy in Japan. Am J Ophthalmol 2004; 137:1081-4. [PMID: 15183793]
18. Oura Y, Kohji N, Yuichi H, Naoyuki M, Tano Y. Phototherapeutic keratectomy and use of extended-wear therapeutic soft contact lenses for the treatment of gelatinous drop-like corneal dystrophy. Nippon Ganka Kiyo 2007; 58:384-8.
19. Kinoshita S, Nishida K, Dota A, Inatomi T, Koizumi N, Elliott A, Lewis D, Quantock A, Fullwood N. Epithelial barrier function and ultrastructure of gelatinous drop-like corneal dystrophy. Cornea 2000; 19:551-5. [PMID: 10928776]
20. Quantock AJ, Nishida K, Kinoshita S. Histopathology of recurrent gelatinous drop-like corneal dystrophy. Cornea 1998; 17:215-21. [PMID: 9520202]
21. Takaoka M, Nakamura T, Ban Y, Kinoshita S. Phenotypic investigation of cell junction-related proteins in gelatinous drop-like corneal dystrophy. Invest Ophthalmol Vis Sci 2007; 48:1095-101. [PMID: 17325151]
22. Nakatsukasa M, Kawasaki S, Yamasaki K, Fukuoka H, Matsuda A, Tsujikawa M, Tanioka H, Nagata-Takaoka M, Hamuro J, Kinoshita S. Tumor-associated calcium signal transducer 2 is required for the proper subcellular localization of claudin 1 and 7: implications in the pathogenesis of gelatinous drop-like corneal dystrophy. Am J Pathol 2010; 177:1344-55. [PMID: 20651236]
23. Ladwein M, Pape UF, Schmidt DS, Schnolzer M, Fiedler S, Langbein L, Franke WW, Moldenhauer G, Zoller M. The cell-cell adhesion molecule EpCAM interacts directly with the tight junction protein claudin-7. Exp Cell Res 2005; 309:345-57. [PMID: 16054130]
24. Tsujikawa K, Tsujikawa M, Yamamoto S, Fujikado T, Tano Y. Allelic homogeneity due to a founder mutation in Japanese patients with lattice corneal dystrophy type IIIA. Am J Med Genet 2002; 113:20-2. [PMID: 12400061]
25. Tsujikawa K, Tsujikawa M, Watanabe H, Maeda N, Inoue Y, Fujikado T, Tano Y. Allelic homogeneity in Avellino corneal dystrophy due to a founder effect. J Hum Genet 2007; 52:92-7. [PMID: 17096061]
26. Fukuoka H, Kawasaki S, Yamasaki K, Matsuda A, Fukumoto A, Murakami A, Kinoshita S. Lattice corneal dystrophy type IV (p.Leu527Arg) is caused by a founder mutation of the TGFBI gene in a single Japanese ancestor. Invest Ophthalmol Vis Sci 2010; 51:4523-30. [PMID: 20357204]

Articles are provided courtesy of Emory University and the Zhongshan Ophthalmic Center, Sun Yat-sen University, P.R. China. The print version of this article was created on 14 April 2011. This reflects all typographical corrections and errata to the article through that date. Details of any changes may be found in the online version of the article.

LETTER

Filaggrin mutations are not associated with chronic allergic keratoconjunctivitis

Filaggrin gene mutations are predisposing genetic factors for atopic dermatitis (AD).[1] In this study, we investigated the association between atopic keratoconjunctivitis (AKC)/vernal keratoconjunctivitis (VKC) and filaggrin gene mutations using a Japanese population. Detailed information on the diagnostic criteria for AKC and VKC was provided elsewhere.[2] The mean age of VKC patients was 15.7±8.9 years (7–32 years), that of AKC patients 28.34±9.9 years (6–50 years) and for controls 42.7±24.3 years (23–67 years). The male:female ratios were 3.2:1.0 for VKC, 3.9:1.0 for AKC and 1:1 for controls.

Four common filaggrin gene mutations in the Japanese population (S2554X, S2889X, S3296X, 3321delA)[3] were genotyped using DNA samples obtained from 69 cases (AKC 44; VKC 25) enrolled in this study. Ninety-three DNA samples obtained from healthy controls (from Health Science Research Resources Japan, Osaka, Japan) were also genotyped. Direct sequence analysis was carried out by dye-terminator methods. Filaggrin gene messenger RNA expression in cultured conjunctival epithelial cells[4] was examined by reverse transcription PCR. Total RNA was extracted and reverse transcription was carried out using random hexamers. We designed PCR primers at the boundary region of exons 2 and 3 of the filaggrin gene (forward 5′–TGCCATAATTAATCTTTTCAAGCA–3′, reverse 5′–TGCTTTCTGTGCTTGTGTCC–3′).

For immunohistological analysis, the giant papillae (n=4) were fixed with 4% paraformaldehyde and paraffin sections were made. A mouse anti-filaggrin gene monoclonal antibody (clone SPM182) purchased from AnaSpec, Inc (San Jose, California, USA) and mouse control IgG1 from Dako Japan (Kyoto, Japan) were used as primary antibodies. Biotin-conjugated goat anti-mouse IgG (Dako) was used as the secondary antibody and then, after incubation with streptoavidin-peroxidase, the positive filaggrin gene signals were visualised using 3,3′-diaminobenzidine, followed by counterstaining with haematoxylin. Normal skin tissues from eyelids (n=4) obtained during ptosis surgery were also stained as a positive control. All procedures were approved by the ethics committees of Juntendo University and Kyoto Prefectural University of Medicine, and this study was conducted in accordance with the tenets of the Declaration of Helsinki.

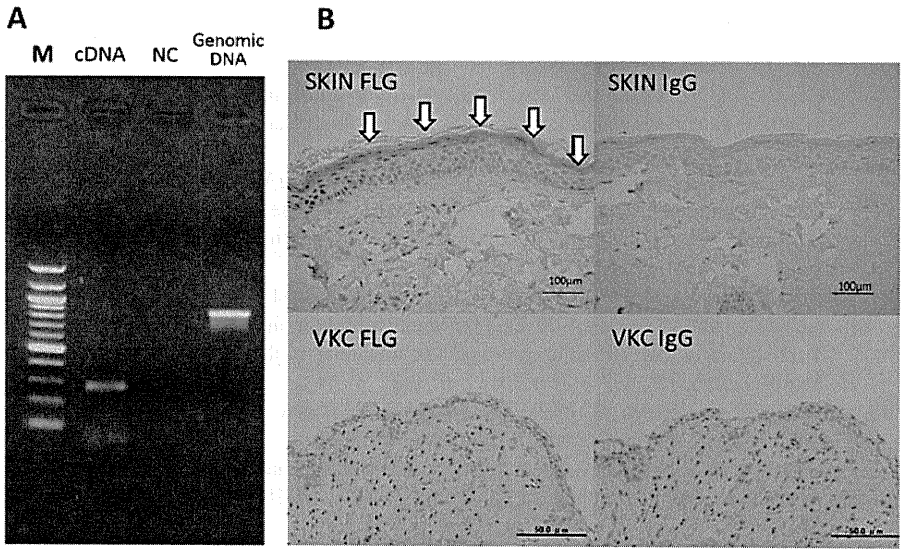

Figure 1 (A) Reverse transcription (RT) PCR analysis of filaggrin gene (FLG) mRNA expression in cultured human conjunctival cells (HCjE). RT–PCR was performed with HCjE complementary DNA, negative control (NC; HCjE sample without reverse transcriptase) and genomic DNA from HCjE. Filaggrin gene mRNA yielded a band at 285 bp; the genomic filaggrin gene sequence yielded a band at 870 bp. M, 100 bp DNA ladder marker. (B) Immunohistochemical analysis of normal eyelid skin (SKIN) and giant papilla tissue from a vernal keratoconjunctivitis (VKC) patient. Positive filaggrin gene immunostaining was observed in the cornified layer of the skin (arrows, FLG SKIN). No positive filaggrin gene staining was observed in VKC samples (FLG VKC). Negative control staining with control IgG is also shown (SKIN IgG and VKC IgG).

Our results revealed no significant association between filaggrin gene mutations and chronic allergic keratoconjunctivitis (table 1). The two patients with the S2554X mutation both had AKC. The patient with the S3296X mutation had VKC. We also carried out statistical comparison between filaggrin gene mutations and AKC (chronic allergic keratoconjunctivitis with AD), but found no association.

As the filaggrin gene mutation spectrum is completely different from those in the Caucasian population, we genotyped the four most common filaggrin gene mutations among Japanese.[3] We also tried to clarify filaggrin gene mRNA and protein expression using conjunctival epithelial cells and tissue. Although we detected filaggrin gene mRNA expression in conjunctival epithelial cells (figure 1A), no filaggrin gene protein expression was observed in conjunctival tissue by immunohistochemistry (figure 1B). These results are consistent with the results of Ying *et al*,[5] in which positive filaggrin gene protein expression was observed in human skin but not in bronchial epithelium, and of Nakamura *et al*[6] showing filaggrin gene protein expression in cicatrising ocular surface diseases but not in normal conjunctivae. The negative association between filaggrin gene mutations and chronic allergic conjunctivitis and lack of filaggrin gene protein expression in VKC/AKC suggested that filaggrin gene mutations did not exert organ-specific effects on the pathophysiology of allergic conjunctivitis in the ocular surface. These results are consistent with the results of Osawa *et al*,[3] which showed genetic association between

Table 1 Genotyping of filaggrin gene mutation for chronic allergic conjunctivitis

	S2554X		S3296X		S2889X		3321delA	
Genotype	control	AKC/VKC	control	AKC/VKC	control	AKC/VKC	control	AKC/VKC
AA	89	67	93	68	93	69	93	69
Aa	4	2	0	1	0	0	0	0
aa	0	0	0	0	0	0	0	0
Totals	93	69	93	69	93	69	93	69
χ^2	p=0.64		p=0.24		NA		NA	

p, p Value of χ^2 test for dominant models (AA vs Aa + aa).
The two patients with the S2554X mutation were atopic keratoconjunctivitis (AKC) patients, and the patient with the S3296X mutation was a vernal keratoconjunctivitis (VKC) patient.
NA, not applicable.

filaggrin gene mutations and asthma with AD but not for asthma without AD.

In summary, we could not detect a positive association between filaggrin gene mutations and chronic allergic keratoconjunctivitis in the Japanese study population. Due to the small size of this genetic association study, replication studies using both oriental and Caucasian populations will be essential to draw firm conclusions.

Acknowledgements The authors would like to thank Professor Ilene K Gipson for providing human conjunctival epithelial cells and Professor Shigeru Kinoshita for clinical sample collection.

Satoshi Iwamoto,[1] Nobuyuki Ebihara,[1] Kanji Hori,[1] Toshinari Funaki,[1] Yosuke Asada,[1] Norihiko Yokoi,[2] Tsutomu Inatomi,[2] Satoshi Kawasaki,[2] Akira Murakami,[1] Akira Matsuda[1]

[1]Department of Ophthalmology, Juntendo University School of Medicine, Tokyo, Japan; [2]Department of Ophthalmology, Kyoto Prefectural University of Medicine, Kyoto, Japan

Correspondence to Dr Akira Matsuda, Department of Ophthalmology, Juntendo University School of Medicine, 2-1-1, Hongo, Bunkyo-Ku, Tokyo 113-8431, Japan; akimatsu@juntendo.ac.jp

Contributors SI, KH and YA performed experiments. NE, TF, NY, TI and SK collected clinical samples and analysed the data. AMu obtained the grant and wrote the paper. AMa planned the experiments, analysed the data, obtained the grant and wrote the paper.

Funding This study was supported by grants-in-aid from MEXT Japan (nos 21592239 and 24592652 to AMa, and no 24659768 to AMu).

Competing interests None.

Ethics approval Ethics approval was provided by Juntendo University and Kyoto Prefectural University.

Provenance and peer review Not commissioned; internally peer reviewed.

Br J Ophthalmol 2012;■:1—2.
doi:10.1136/bjophthalmol-2012-301990

REFERENCES

1. **Palmer CN,** Irvine AD, Terron-Kwiatkowski A, *et al*. Common loss-of-function variants of the epidermal barrier protein filaggrin are a major predisposing factor for atopic dermatitis. *Nat Genet* 2006;**38**:441—6.
2. **Matsuda A,** Okayama Y, Ebihara N, *et al*. Hyperexpression of the high-affinity IgE receptor-beta chain in chronic allergic keratoconjunctivitis. *Invest Ophthalmol Vis Sci* 2009;**50**:2871—7.
3. **Osawa R,** Konno S, Akiyama M, *et al*. Japanese-specific filaggrin gene mutations in Japanese patients suffering from atopic eczema and asthma. *J Invest Dermatol* 2010;**130**:2834—6.
4. **Gipson IK,** Spurr-Michaud S, Argueso P, *et al*. Mucin gene expression in immortalized human corneal—limbal and conjunctival epithelial cell lines. *Invest Ophthalmol Vis Sci* 2003;**44**:2496—506.
5. **Ying S,** Meng Q, Corrigan CJ, *et al*. Lack of filaggrin expression in the human bronchial mucosa. *J Allergy Clin Immunol* 2006;**118**:1386—8.
6. **Nakamura T,** Nishida K, Dota A, *et al*. Elevated expression of transglutaminase 1 and keratinization-related proteins in conjunctiva in severe ocular surface disease. *Invest Ophthalmol Vis Sci* 2001;**42**:549—56.

Involvement of Plasminogen Activator Inhibitor-1 in the Pathogenesis of Atopic Cataracts

Kanji Hori,[1] Akira Matsuda,[1] Nobuyuki Ebihara,[1] Kojiro Imai,[2] Kazuhiko Mori,[2] Toshinari Funaki,[1] Yasuo Watanabe,[1] Satoru Nakatani,[1] Kiyotaka Okada,[3] Osamu Matsuo,[3] and Akira Murakami[1]

Purpose. Further to our previous report of a genetic association between interferon-gamma (IFN-γ) receptor 1 gene and atopic cataract, we investigated the roles of plasminogen activator inhibitor-1 (PAI-1), a fibrosis-related, IFN-γ downstream molecule, in the pathogenesis of atopic cataracts.

Methods. Cultured lens epithelial cells (LECs) were stimulated by IFN-γ and quantified by PAI-1 mRNA/protein expression. PAI-1 and TGF-β mRNA expression was quantified using cDNA samples obtained from the lens epithelium of atopic cataract patients ($n = 7$) and of senile cataract patients ($n = 8$). The anterior capsules obtained from atopic cataracts ($n = 9$) were immunostained with anti-PAI-1 and anti-alpha smooth muscle actin (α-SMA) antibodies. PAI-1 gene expression was knocked down by PAI-1 siRNA, and α-SMA expression was examined under TGF-β1 stimulation. Expression of α-SMA was examined as a pathological hallmark of anterior subcapsular cataracts, commonly observed in atopic cataracts.

Results. The IFN-γ stimulation induced PAI-1 mRNA/protein expression in the LECs from 24 to 48 hours after stimulation. The expression of PAI-1 mRNA and TGF-β1 mRNA was significantly higher in the cDNA samples obtained from the atopic cataracts than those obtained from the senile cataracts. PAI-1-positive immunostaining was observed at the fibrotic lesion of the atopic cataracts, and α-SMA-positive myofibroblasts were observed at the vicinity of the PAI-1-positive lesion in all nine samples examined. PAI-1 gene knockdown resulted in reduced α-SMA expression in the LECs.

Conclusions. The findings of this study suggest that the IFN-γ, PAI-1, and TGF-β1 are involved in the pathophysiology of atopic cataracts. (*Invest Ophthalmol Vis Sci.* 2012;53:1846–1851) DOI:10.1167/iovs.11-8380

From the [1]Department of Ophthalmology, Juntendo University School of Medicine, Tokyo, Japan; the [2]Department of Ophthalmology, Kyoto Prefectural University of Medicine, Kyoto, Japan; and the [3]Department of Physiology, Kinki University School of Medicine, Sayama, Japan.

Supported by Grant-in-Aids No. 19659454 (AMu) and No. 18604009 (AMa) from Ministry of Education, Culture, Sports, Science and Technology (MEXT) Japan.

Submitted for publication August 8, 2011; revised January 7, February 13, 2012, and February 15, 2012; accepted February 15, 2012.

Disclosure: **K. Hori**, None; **A. Matsuda**, None; **N. Ebihara**, None; **K. Imai**, None; **K. Mori**, None; **T. Funaki**, None; **Y. Watanabe**, None; **S. Nakatani**, None; **K. Okada**, None; **O. Matsuo**, None; **A. Murakami**, None

Corresponding author: Akira Matsuda, Department of Ophthalmology, Juntendo University School of Medicine, 2-1-1 Hongo, Bunkyo-Ku, Tokyo, 113-8431, Japan; akimatsu@juntendo.ac.jp.

Investigative Ophthalmology & Visual Science, April 2012, Vol. 53, No. 4

Atopic cataracts are atopic-disease-related complications that typically affect individuals in their adolescent years.[1] Treatment of atopic cataracts usually requires cataract surgery that results in a loss of patient's natural power of accommodation. In some cases, a subsequent retinal detachment is also observed.[2] In a previous study, we reported an association between interferon-gamma (IFN-γ) receptor genetic polymorphisms and the occurrence of atopic cataracts.[3] Atopic cataracts often have the phenotype of anterior subcapsular cataracts, accompanied by abnormal fibrosis and epithelial-to-mesenchymal transition (EMT) of lens epithelial cells (LECs) into myofibroblasts.[4]

In the present study, we focused on several molecules associated with fibrosis and LEC transition. A recent study showed that the IFN-γ signal is essential for plasminogen activator inhibitor (PAI)-1-induced postoperative fibrosis in the abdomen, where PAI-1 expression is upregulated by IFN-γ and STAT1 signal cascades.[5] PAI-1 inhibits urokinase/tissue type plasminogen activator (uPA/tPA) and subsequent plasmin/plasmin-dependent matrix metalloprotease (MMP) activity, thus increasing PAI-1 expression that results in profibrotic collagen/matrix deposition by suppressing fibrinolysis.[6,7]

Reports from other lines of investigation have shown that the overexpression of TGF-β signals in LECs could induce an anterior subcapsular cataract in mice.[8] TGF-β is a typical cytokine related to fibrosis and EMT phenomena. In addition, TGF-β is known to induce PAI-1 expression,[7] and one previous study demonstrated that PAI-1 mediates TGF-β1+ epidermal growth factor-induced EMT.[9] In the present study, we investigated the roles of PAI-1 in association with TGF-β in the formation of atopic cataracts.

Materials and Methods

Clinical Samples

Anterior capsules from 16 atopic-cataract and 8 senile-cataract patients were obtained at the time of surgery as previously described.[3] All the atopic cataracts patients were diagnosed by slit-lamp analysis by board-certificated ophthalmologists, and atopic dermatitis of these patients was diagnosed according to the criteria of Hanifin and Rajka.[10] Nine samples of atopic cataract were processed for immunofluorescence analyses and seven atopic cataract samples, along with senile cataracts, were used for isolation of RNA for real-time PCR experiments. Written informed consent was obtained from all patients prior to surgery. All procedures were approved by the Ethics Committees of Juntendo University School of Medicine and Kyoto Prefectural University of Medicine, and the study was conducted in accordance with the tenets of the Declaration of Helsinki.

Antibodies and Reagents

Goat anti-PAI-1 polyclonal antibody was purchased from R&D Systems, Inc. (Minneapolis, MN), mouse anti-human α-SMA monoclonal

antibody from Dako Japan (Kyoto, Japan), and rabbit anti-human α-SMA monoclonal antibody from Epitomics (Burlingame, CA). Recombinant human TGF-β1 and IFN-γ protein were obtained from PeproTech Ltd. (London, UK), and pEF6-V5-His plasmid from Life Technologies (Carlsbad, CA). All other reagents used in this study were analytical grade reagents.

LEC Culture with IFN-γ Stimulation, Anterior Lens Capsules Collection, and cDNA Preparation

Human immortalized LECs (SRA01/04) obtained from RIKEN cell bank (Tsukuba, Japan) were maintained with 10% fetal bovine serum (FBS) in MEM (Life Technologies).[11] Subconfluent LECs in 12-well cell culture dishes were stimulated with IFN-γ (20 ng/mL) for 24 and 48 hours.

Anterior lens capsules obtained during cataract surgery were immediately stored with RNA Later (Ambion, Austin, TX) to protect the RNA. Total RNA was extracted from the LECs with a NucleoSpin II RNA Isolation Kit (Macherey-Nagel GmbH, Duren, Germany), and from the anterior capsules by use of the Micro RNA Extraction Kit (Qiagen Japan, Tokyo, Japan). cDNAs were prepared using random primers and ReverTra Ace reverse transcriptase (both from Toyobo, Osaka, Japan) according to the manufacturer's protocol.

Real-Time PCR Analysis

Real-time PCR was carried out using human PAI-1 (Hs00167155_m1), TGF-β1 (Hs00998130_m1), TGF-β2 (Hs00234244_m1), and 18S-rRNA (4319413E) TaqMan Expression Assay (Assays-on-Demand gene expression products) with TaqMan Fast Master Mix. Expression of α-SMA was quantified using Fast SYBR Green Master Mix with a pair of primers (Forward 5′-CCCAGCCAAGCACTGTCA-3′; Reverse 5′-TCCAGAGTCCAGCACGATG-3′). Real-time PCR analysis was carried out on a PRISM 7500 Sequence Detection System (all from Life Technologies). The relative expression of PAI-1 in LECs was quantified by the standard curve method using full-length PAI-1 cDNA subcloned into the pEF6-V5-His plasmid as standard and 18S-rRNA expression in the same cDNA as the control. Relative expression of α-SMA, TGF-β1, and TGF-β2 was quantified by comparative Ct methods using 18S-rRNA expression in the same cDNA as the control.

Immunohistochemistry and Electron Microscopy

Lens capsules obtained at the time of cataract surgery were fixed in 4% paraformaldehyde/PBS and then embedded in paraffin, and 3-μm paraffin sections were then made and used for the immunohistologic analysis. For some experiments, the fixed lens capsules were immunostained as whole-mount samples. Nonspecific staining was blocked for 30 minutes with blocking buffer (10% normal donkey serum, and 1% BSA in PBS). Goat anti-PAI-1 polyclonal antibody (1:200 dilution) or mouse anti-α-SMA (1:100 dilution) was then applied and reacted overnight at 4°C. All the antibodies were diluted with the blocking buffer. After washing with PBS, the slides were incubated for 30 minutes with Alexa 488–conjugated donkey anti-mouse IgG or with Alexa 594–conjugated anti-goat IgG (both from Life Technologies). The slides were then inspected by the use of a confocal microscope (TCS SP5; Leica Microsystems, Tokyo, Japan). Ultrastructural analysis was carried out essentially as previously described.[12] Lens capsules obtained at the time of cataract surgery were immediately fixed with 2.5% glutaraldehyde and then postfixed with 2% osmic acid. The samples were embedded in epoxy resin and ultrathin sections (60–80 nm) were then made. The ultrathin sections were examined by use of a transmission electron microscope (7000-100; Hitachi High-Technologies, Inc., Tokyo, Japan).

PAI-1 Gene Knockdown in LECs

First, LECs in the 24-well cell dishes were stimulated with 20 ng/mL human TGF-β1 and chronological change of PAI-1/α-SMA mRNA was examined. A PAI-1 gene knockdown experiment was performed with MISSION esiRNA against PAI-1 (EHU016891), and esiRNA against Renilla luciferase (RLUC, negative control), using the N-TER Nanoparticle siRNA Transfection System (both from Sigma-Aldrich, St. Louis, MO) according to the manufacturer's protocol. In each well of a 24-well cell culture dish, 500 ng of siRNA was used with 1.6 μL N-TER reagents for transfection. The LECs in the 24-well cell dishes were then stimulated with 0.2 ng/mL human TGF-β1, immediately after the transfection procedures. cDNAs were prepared from total RNA, and PAI-1 mRNA and α-SMA mRNA expression was quantified by real-time PCR as described above.

Western Blot Analysis

Western blotting analysis was carried out essentially as previously described.[13] In brief, LECs in the 12-well culture dish were washed twice with PBS. Cells in the amount of 4×10^4 were then solubilized in SDS-sample buffer (62.5 mM Tris-HCl, pH 6.8, 2% SDS, 20% glycerol, and 0.04% bromophenol blue). Next, 50 mM dithiothreitol (DTT) was added to the samples and incubated for 15 minutes at 95°C. Of each sample, 12 μL was loaded with 4% to 20% gradient Tris-glycine gel. The electrophoresed protein was transferred to a polyvinylidene fluoride (PVDF) membrane (Pall Japan, Tokyo, Japan), and the membrane was then incubated with the goat anti- PAI-1 polyclonal antibody (1:5000 dilution) or with the rabbit anti-α-SMA monoclonal antibody (1:3000 dilution) overnight at 4°C. After washing with Tris-buffered saline (10 mM Tris-HCl, pH 7.6, 150 mM NaCl) containing 0.05% Tween 20 (TBS-T), the membrane was incubated with a 1:10,000 dilution of horse radish peroxidase (HRP)-conjugated anti-rabbit IgG (GE Healthcare, Uppsala, Sweden) or HRP-conjugated anti-goat IgG (Jackson Immuno Research Lab Inc., West Grove, PA) for 1 hour and then visualized with ECL Plus Western blotting reagents (GE Healthcare). The density of PAI-1/α-SMA positive bands was quantified by ImageJ software (ImageJ software, http://rsbweb.nih.gov/ij/, NIH).

Results

IFN-γ Stimulation-Induced PAI-1 mRNA and Protein Up-Regulation

Recombinant IFN-γ stimulation (20 ng/mL) induced a 4.6-fold increase in PAI-1 mRNA expression in the cultured LECs at 48 hours after stimulation (Fig. 1A). Immunocytochemical staining of the LECs showed increased PAI-1 protein expression at 24 and 48 hours after stimulation (Fig. 1B). PAI-1 Western blot analysis of the IFN-γ (20 ng/mL) stimulated LECs showed increased PAI-1 expression at 24 and 48 hours after stimulation (Fig. 1C). A 6.3-fold increase in PAI-1 protein expression was observed in the LECs after 48 hours.

Increased PAI-1 mRNA Expression in the Lens Epithelial Cells Obtained from Atopic Cataracts

The relative expression of PAI-1 mRNA was significantly higher in the cDNA samples obtained from atopic cataracts compared with those from senile cataracts (Fig. 2A). TGF-β1 mRNA expression was also significantly higher in the atopic samples (Fig. 2B), whereas no significant difference was observed in regard to TGF-β2 expression (Fig. 2C). Statistical analysis was carried out by use of the Mann-Whitney *U* test.

PAI-1 Protein Was Deposited at the Subcapsular Fibrotic Region of Atopic Cataracts

PAI-1–positive immunostaining was observed at the subcapsular fibrotic lesion of the atopic cataracts (Fig. 3A, red color). A negative control section incubated with normal goat IgG did

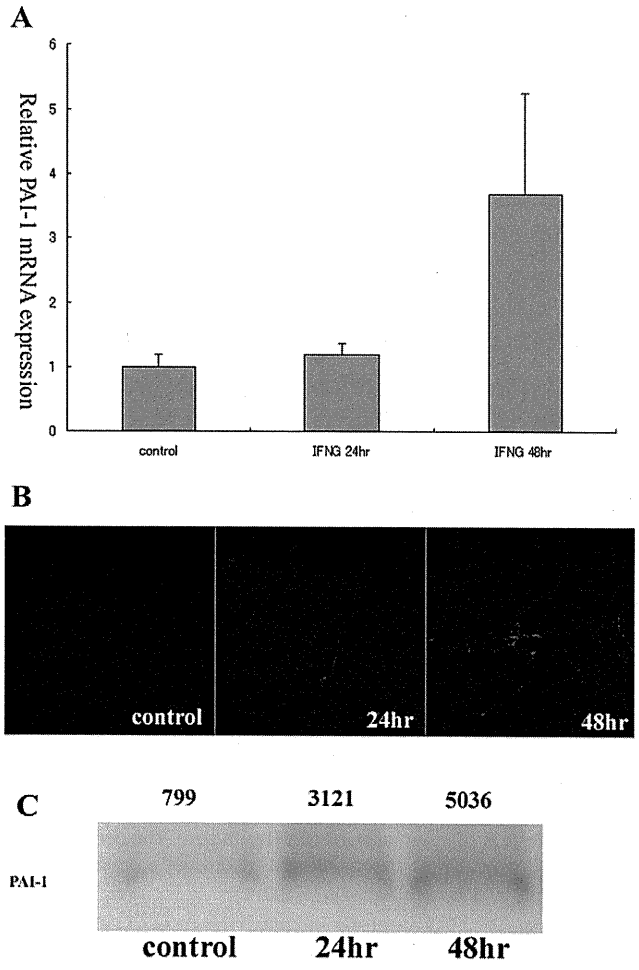

FIGURE 1. The effect of recombinant IFN-γ stimulation for PAI-1 mRNA and protein expression in LECs. (**A**) Real-time PCR analysis of PAI-1 mRNA expression. LECs were stimulated with 20 ng/mL IFN-γ for 24 and 48 hours. The results are shown as mean-fold ± SD compared with PAI-1 mRNA expression of the unstimulated sample. (**B**) Immunocytochemical staining of LECs with PAI-1 antibody (red). Note the positive staining between the junctions of the LECs at 24 and 48 hours after IFN-γ stimulation. The nuclei of the LECs were counterstained with DAPI. (**C**) Western blot analysis of PAI-1 protein expression. LECs were stimulated with 20 ng/mL IFN-γ for 24 and 48 hours. Western blot analysis was carried out using goat anti-PAI-1 antibody. The density of PAI-1–positive bands is shown on the top of each band.

not exhibit positive staining (Fig. 3B). α-SMA–positive myofibroblastic cells were observed in the vicinity of the PAI-1–positive deposits in the fibrotic region of the atopic cataracts. Whole-mount PAI-1 immunostaining showed positive immunostaining within and around LECs of the subcapsular cataract region (Fig. 3C); however, LECs at the non-cataractous clear region did not exhibit any PAI-1–positive staining (Fig. 3D). Ultrastructural analysis showed a structureless deposit between the irregular LECs and the basement membrane (Fig. 3E, asterisk). The clear region in the same lens capsule showed a monolayer of LECs (Fig. 3F). The results of PAI-1 immunostaining using nine anterior capsule samples obtained from the atopic cataract patients are summarized in Table 1. All the

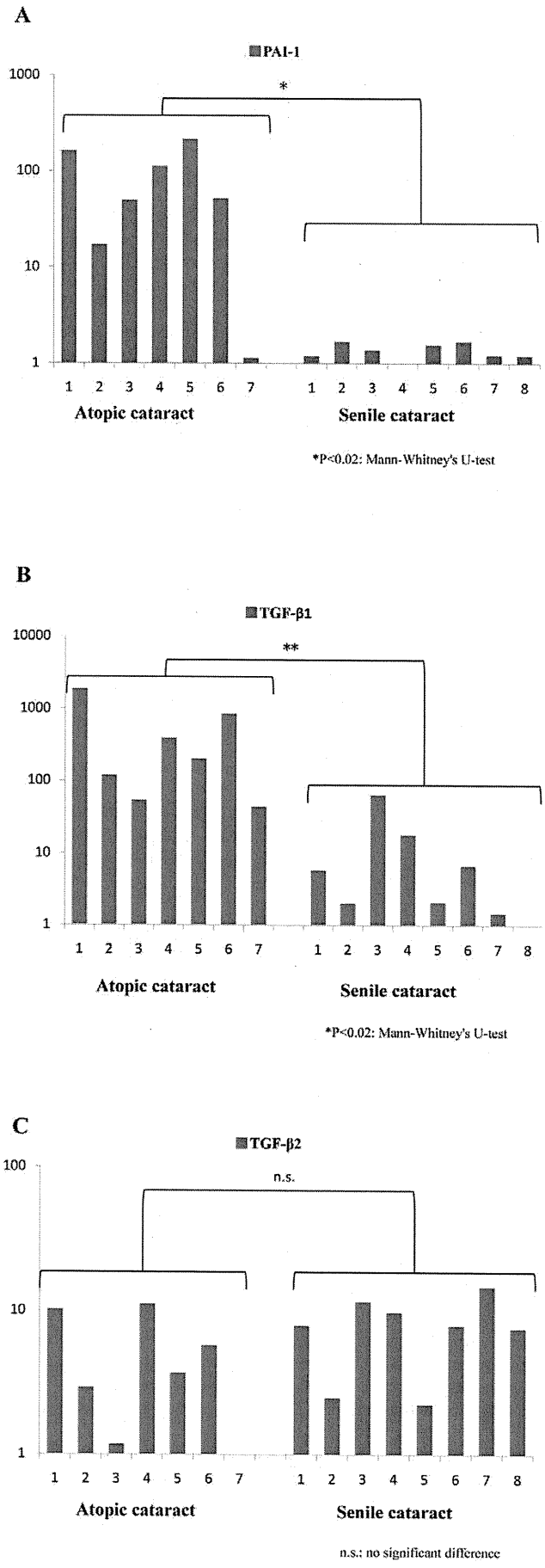

FIGURE 2. Real-time PCR analysis of (**A**) PAI-1, (**B**) TGF-β1, and (**C**) TGF-β2 mRNA expression in human anterior lens capsules. The amount of relative expression was normalized to that of 18S rRNA.

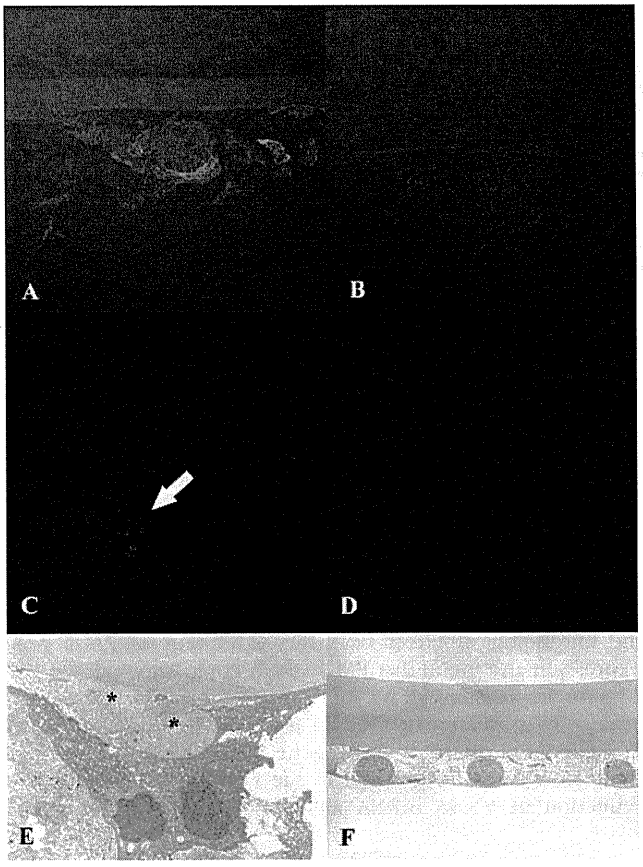

FIGURE 3. Immunohistochemical staining of human anterior lens capsules with the anti-PAI-1 antibody. Paraffin sections of the lens capsule were immunostained with (A) goat anti-PAI-1 antibody and mouse anti-α-SMA antibody or with (B) normal goat IgG and normal mouse IgG1. Alexa 594–conjugated anti-goat IgG (red) and Alexa 488–conjugated anti-mouse IgG (green) were used for the secondary antibody. Whole-mount PAI-1 immunostaining of (C) the fibrotic plaque or (D) the clear part of the same anterior lens capsule of an atopic cataract patient. Positive PAI-1 immunostaining (red) was observed around the fibrotic-plaque (C). (A–D) Original magnification ×600. Ultrastructural analysis of LECs in (E) the fibrotic plaque and in (F) the clear part of the anterior lens capsule of an atopic cataract patient. An acellular deposit (asterisk) was observed beneath the epithelial cells with fibrotic morphology (E).

anterior capsules showed positive PAI-1 immunostaining, and the staining was classified as focal, diffuse, and diffuse + focal, as shown in Fig. 4. α-SMA–positive myofibroblastic cells were observed in all samples near the PAI-1–positive fibrotic lesions.

PAI-1 Expression Knockdown Could Suppress TGF-β1–Dependent α-SMA mRNA Expression in the LECs

First, chronological changes of PAI-1 mRNA and α-SMA mRNA in response to TGF-β1 (20 ng/mL) stimulation were evaluated. TGF-β1 stimulation induced PAI-1 mRNA that at first peaked at 8 hours after simulation, followed by α-SMA mRNA being induced from 8 hours after stimulation and peaking at 24 hours after stimulation (Fig. 5). PAI-1 siRNA transfection using unstimulated (without TGF-β1) LECs resulted in 77% knockdown efficiency at 12 hours and 71% knockdown efficiency of PAI-1 mRNA expression at 24 hours after transfection (data not shown). PAI-1 siRNA transfection resulted in 32% knockdown efficiency at 12 hours and 73% knockdown efficiency at 24 hours after siRNA transfection under simultaneous TGF-β1 (0.2 ng/mL) stimulation (Fig. 6A). PAI-1 siRNA transfection suppressed α-SMA expression compared with the control siRNA at 12 hours (60% reduction) to 24 hours (42% reduction) after TGF-β1 stimulation/siRNA transfection (Fig. 6A). Western blot analysis of TGF-β1 (0.2 ng/mL)–stimulated/siRNA transfected LECs showed a 43% reduction of PAI-1 protein expression and a 40% reduction of α-SMA protein expression compared with the RLUC siRNA-transfected control sample (Fig. 6B) at 24 hours after the stimulation/transfection procedures.

TABLE 1. Summary of PAI-1 Immunostaining

Patients	Age	Sex	Affected eye(s)	PAI-1 immunostaining
NO.1	23	F	R	Focal
NO.2	32	M	R	Diffuse
NO.3	31	F	L	Diffuse+Focal
NO.4	28	M	R, L	Diffuse
NO.5	40	M	L	Diffuse+Focal
NO.6	43	M	R, L	Focal
NO.7	18	M	R, L	Diffuse
NO.8	32	M	R, L	Diffuse
NO.9	40	M	R	Diffuse+Focal

DISCUSSION

In our previous study, we showed increased IFN-γ receptor 1 mRNA expression and major histocompatibility complex (MHC) class-II immunostaining in the anterior capsules of atopic cataracts, indicating the relevance of IFN-γ signals for atopic cataract formation.[3] In this present study, we first showed that IFN-γ treatment could up-regulate PAI-1 mRNA/protein expression in LECs (Fig. 1). Considering the previous reports, which showed that STAT1 activation leads to PAI-1 gene promoter up-regulation,[5,14] the effect of IFN-γ treatment is proposed to be indirect and dependent on STAT1 activation. Therefore, a relatively long duration of time (24–48 hours) is required before PAI-1 mRNA/protein induction by IFN-γ (Fig. 1). The roles of the PAI-1 molecule as a profibrotic molecule have been reported in many disease-related systems (e.g., glomerulonephritis,[15] bleomycin-induced pulmonary fibrosis,[16] keloid formation in the skin[17]).

We next showed that significantly higher PAI-1 mRNA (Fig. 2A) and TGF-β1 mRNA (Fig. 2B) expression in atopic cataracts compared with senile cataracts. Suzuki et al. recently reported a significantly higher PAI-1 protein concentration in the aqueous humor of atopic cataracts compared with senile cataracts, which is consistent with the findings of this study.[18] Lee and Joo reported increased TGF-β1 mRNA expression in anterior polar cataracts compared with nuclear cataracts.[19] Although there was no description in that report as to the atopic status of the anterior polar cataracts, our results are in agreement with the finding of that study when considering the common phenotype of the cataracts.[19] It should be noted that atopic cataracts are not necessarily anterior subcapsular cataracts. Nonetheless, the anterior subcapsular cataract is one of the common and specific atopic cataract phenotypes.[20,21]

Immunohistologic analysis showed PAI-1 protein deposition (Fig. 3A, 3C red color) at the fibrotic lesion of the anterior lens capsules in atopic cataracts. Our findings also revealed α-SMA–positive myofibroblastic cells in the lesion of the anterior subcapsular cataracts (Fig. 3A, green color). Furthermore, PAI-1–positive immunostaining and nearby α-SMA–positive myofi-

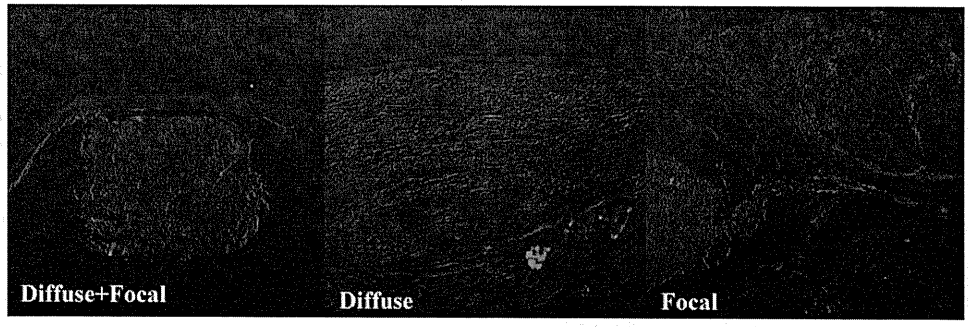

FIGURE 4. Immunohistochemical staining of human anterior lens capsules with the anti-PAI-1 antibody. Paraffin sections of the lens capsule were immunostained with goat anti-PAI-1 (red) antibody and mouse anti-α-SMA (green) antibody. Arrows indicate the focal PAI-1 staining. Staining patterns were classified as diffuse + focal staining, diffuse staining, or focal staining as shown in the Figure. Original magnification ×200.

broblastic cells were found in all nine anterior capsule samples obtained from the atopic cataract patients (Table 1; Fig. 4). These findings are consistent with those of a previous study, which reported that myofibroblast is the predominant PAI-1 expression cell type in human breast carcinomas.[22] Ultrastructural analysis of the atopic cataracts capsule showed myofibroblastic cells at the fibrotic lesion and an abnormal acellular deposit beneath the myofibroblastic cells (Fig. 3E). These results suggest the possibility that PAI-1 protein is deposited around the myofibroblasts of atopic cataracts and may play some role as a scaffold for the EMT phenomenon, as suggested in keratinocyte experimental models.[9] Further immuno-electron microscopic studies are ongoing to show the precise localization of PAI-1 protein in relation to myofibroblastic cells in atopic cataracts.

The results of the PAI-1 gene knockdown experiments using LECs (Fig. 5, 6) also support the roles of PAI-1 for the induction of α-SMA, a pathological hallmark of anterior subcapsular cataracts and EMT.[4] First, we evaluated the chronological changes of PAI-1 mRNA and α-SMA mRNA in response to TGF-β1 stimulation. TGF-β1 stimulation induced PAI-1 mRNA that first peaked at 8 hours after simulation, followed by α-SMA mRNA being induced from 8 hours after stimulation and peaking at 24 hours after stimulation (Fig. 5). In our preliminary experiment, we utilized a relatively high dose of TGF-β1 (20 ng/mL) for the LECs stimulation and found that owing to the very strong effect of TGF-β1 for PAI-1 mRNA induction, knockdown efficiency of PAI-1 siRNA was not sufficient under TGF-β1 stimulation compared with control samples without TGF-β1 stimulation. Thus, we optimized the dose of TGF-β1 stimulation to 0.2 ng/mL. We then evaluated the chronological effect of siRNA inhibition of PAI-1 gene expression and found that PAI-1 siRNA could knock down PAI-1 gene expression at 32% (12 hours) to 73% (24 hours) efficiency post transfection (Fig. 6A). We simultaneously evaluated the effect of PAI-1 gene knockdown for TGF-β1-induced α-SMA up-regulation in the LECs and showed a 42% reduction of α-SMA mRNA and a 40% reduction of α-SMA

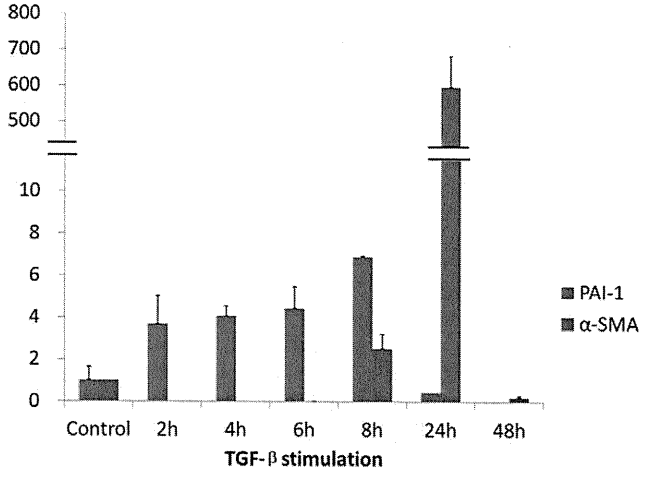

FIGURE 5. Chronological change of PAI-1 and α-SMA mRNA expression in LECs. TGF-β1 (20 ng/mL) treatment induced PAI-1 mRNA up-regulation from 8 hours after stimulation and then triggered α-SMA up-regulation that peaked at 24 hours after stimulation. All results are shown as mean-fold ± SD compared with that of the PAI-1/α-SMA mRNA expression of the untreated sample.

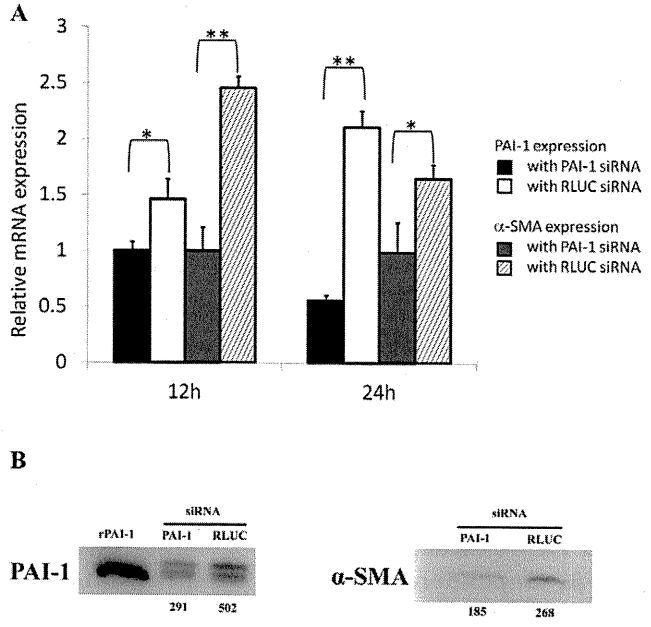

FIGURE 6. PAI-1 gene knockdown suppressed TGF-β1 (0.2 ng/mL)-induced α-SMA expression in the LECs. (**A**) PAI-1 gene knockdown suppressed TGF-β1-induced PAI-1 expression from 12 to 24 hours, compared with the RLUC gene knockdown control, and PAI-1 gene knockdown also inhibited TGF-β1-induced α-SMA expression at 24 hours after stimulation. All results are shown as mean-fold ± SD compared with PAI-1/α-SMA mRNA expression of the PAI-1 siRNA-treated samples at 12 hours after stimulation/transfection (* $P < 0.05$, ** $P < 0.01$, Student's *t*-test). (**B**) Western blot analysis of LECs with PAI-1 gene knockdown under TGF-β1(0.2 ng/mL) stimulation. PAI-1 and α-SMA Western blot analysis was carried out. Recombinant rPAI-1 (5 ng/mL) was loaded as a control. The density of PAI-1/α-SMA-positive bands is shown at the bottom of each band.

protein expression at 24 hours (Fig. 6A). These results support our hypothesis that PAI-1 may play a role for scaffold protein for α-SMA expression and subsequent EMT in LECs.

In summary, our findings demonstrated that IFN-γ could induce PAI-1 expression in LECs, PAI-1 protein expression at the vicinity of α-SMA-positive myofibroblasts in atopic cataracts, and the essential roles of PAI-1 for α-SMA expression of LECs under TGF-β1 stimulation. These results suggest that IFN-γ, PAI-1, and TGF-β1 all play significant roles in the pathophysiology of atopic cataracts. Previous studies have shown several roles of the PAI-1 molecule in atopy-related disorders. Oh et al. reported that PAI-1 promotes extracellular matrix deposition in the airway of mouse asthma models.[23] Sejima et al. reported the role of PAI-1 in an ovalbumin (OVA)-induced nasal allergy model, showing decreased eosinophil infiltration, goblet cell hyperplasia, and Th2-skew immune responses in the PAI-1 knockout mouse.[24] These results are consistent to our results showing increased PAI-1 expression and essential roles of PAI-1 in the pathophysiology of atopic cataracts. Further investigations are currently being conducted to elucidate methods for preventing the development of atopic cataracts by intervening in the PAI-1–induced fibrotic cascades.

Acknowledgments

The authors thank Julian M. Hopkin and Shigeru Kinoshita for their invaluable continuous support.

References

1. Uehara M, Amemiya T, Arai M. Atopic cataracts in a Japanese population. With special reference to factors possibly relevant to cataract formation. *Dermatologica.* 1985;170:180–184.
2. Hida T, Tano Y, Okinami S, Ogino N, Inoue M. Multicenter retrospective study of retinal detachment associated with atopic dermatitis. *Jpn J Ophthalmol.* 2000;44:407–418.
3. Matsuda A, Ebihara N, Kumagai N, et al. Genetic polymorphisms in the promoter of the interferon gamma receptor 1 gene are associated with atopic cataracts. *Invest Ophthalmol Vis Sci.* 2007;48:583–589.
4. Schmitt-Graff A, Pau H, Spahr R, Piper HM, Skalli O, Gabbiani G. Appearance of alpha-smooth muscle actin in human eye lens cells of anterior capsular cataract and in cultured bovine lens-forming cells. *Differentiation.* 1990;43:115–122.
5. Kosaka H, Yoshimoto T, Yoshimoto T, Fujimoto J, Nakanishi K. Interferon-gamma is a therapeutic target molecule for prevention of postoperative adhesion formation. *Nat Med.* 2008;14:437–441.
6. Eddy AA, Fogo AB. Plasminogen activator inhibitor-1 in chronic kidney disease: evidence and mechanisms of action. *J Am Soc Nephrol.* 2006;17:2999–3012.
7. Ghosh AK, Vaughan DE. PAI-1 in tissue fibrosis. *J Cell Physiol.* 2011;227:493–507.
8. Lovicu FJ, Schulz MW, Hales AM, et al. TGFbeta induces morphological and molecular changes similar to human anterior subcapsular cataract. *Br J Ophthalmol.* 2002;86:220–226.
9. Freytag J, Wilkins-Port CE, Higgins CE, Higgins SP, Samarakoon R, Higgins PJ. PAI-1 mediates the TGF-beta1+EGF-induced "scatter response in transformed human keratinocytes." *J Invest Dermatol.* 2011;130:2179–2190.
10. Hanifin JM, Rajka RG. Diagnostic features of atopic dermatitis. *Acta Derm Venereol.* 1980;92(suppl);44–47.
11. Ibaraki N, Chen SC, Lin LR, Okamoto H, Pipas JM, Reddy VN. Human lens epithelial cell line. *Exp Eye Res.* 1998;67:577–585.
12. Matsuda A, Ebihara N, Yokoi N, et al. Basophils in the giant papillae of chronic allergic keratoconjunctivitis. *Br J Ophthalmol.* 2010;94:513–518.
13. Matsuda A, Okayama Y, Terai N, et al. The role of interleukin-33 in chronic allergic conjunctivitis. *Invest Ophthalmol Vis Sci.* 2009;50:4646–4652.
14. Kasza A, Kiss DL, Gopalan S, et al. Mechanism of plasminogen activator inhibitor-1 regulation by oncostatin M and interleukin-1 in human astrocytes. *J Neurochem.* 2002;83:696–703.
15. Kitching AR, Holdsworth SR, Ploplis VA, et al. Plasminogen and plasminogen activators protect against renal injury in crescentic glomerulonephritis. *J Exp Med.* 1997;185:963–968.
16. Eitzman DT, McCoy RD, Zheng X, et al. Bleomycin-induced pulmonary fibrosis in transgenic mice that either lack or overexpress the murine plasminogen activator inhibitor-1 gene. *J Clin Invest.* 1996;97:232–237.
17. Tuan TL, Hwu P, Ho W, et al. Adenoviral overexpression and small interfering RNA suppression demonstrate that plasminogen activator inhibitor-1 produces elevated collagen accumulation in normal and keloid fibroblasts. *Am J Pathol.* 2008;173:1311–1325.
18. Suzuki S, Sagara H, Senoo T. Developmental Factors of Fibrous Opacification in the Atopic Cataract Lens Capsule. *Ophthalmic Res.* 2011;45:216–220.
19. Lee EH, Joo CK. Role of transforming growth factor-beta in transdifferentiation and fibrosis of lens epithelial cells. *Invest Ophthalmol Vis Sci.* 1999;40:2025–2032.
20. Bair B, Dodd J, Heidelberg K, Krach K. Cataracts in atopic dermatitis: a case presentation and review of the literature. *Arch Dermatol.* 2011;147:585–588.
21. Fagerholm P, Palmquist BM, Philipson B. Atopic cataract: changes in the lens epithelium and subcapsular cortex. *Graefes Arch Clin Exp Ophthalmol.* 1984;221:149–152.
22. Offersen BV, Nielsen BS, Hoyer-Hansen G, et al. The myofibroblast is the predominant plasminogen activator inhibitor-1-expressing cell type in human breast carcinomas. *Am J Pathol.* 2003;163:1887–1899.
23. Oh CK, Ariue B, Alban RF, Shaw B, Cho SH. PAI-1 promotes extracellular matrix deposition in the airways of a murine asthma model. *Biochem Biophys Res Commun.* 2002;294:1155–1160.
24. Sejima T, Madoiwa S, Mimuro J, et al. Protection of plasminogen activator inhibitor-1-deficient mice from nasal allergy. *J Immunol.* 2005;174:8135–8143.

Perlecan-Deficient Mutation Impairs Corneal Epithelial Structure

Takenori Inomata,[1,2] *Nobuyuki, Ebihara,*[1] *Toshinari Funaki,*[1] *Akira Matsuda,*[1] *Yasuo Watanabe,*[1] *Liang Ning,*[2] *Zhuo Xu,*[2] *Akira Murakami,*[1] *and Eri Arikawa-Hirasawa*[2,3]

Purpose. To elucidate the role of perlecan (Hspg2), a large multidomain heparan sulfate proteoglycan expressed in the basement membrane, in the structure of the corneal epithelium.

Methods. A previously developed perlecan-deficient (*Hspg2*$^{-/-}$-Tg) mouse model was used. Histologic analysis of their corneas was performed by light and transmission electron microscopy. The localization of perlecan in the corneas of wild-type (WT) mice and *Hspg2*$^{-/-}$-Tg mice was examined by immunohistochemistry. The effects of perlecan deficiency on corneal epithelial structure was analyzed with respect to the expression of corneal epithelial proliferation and differentiation markers, such as Ki67, cytokeratin12 (K12), connexin43 (Cx43), Notch1, and Pax6 by immunohistochemistry and real-time polymerase chain reaction (PCR).

Results. The *Hspg2*$^{-/-}$-Tg mice had microphthalmos and a thinner corneal epithelium compared with that of the WT mice. Perlecan was localized in the corneal epithelial basement membrane in the WT mice, but not in the *Hspg2*$^{-/-}$-Tg mice. The *Hspg2*$^{-/-}$-Tg corneal epithelium exhibited thinner wing cell layers and a decreased number of Ki67-positive cells, but no dead cells, compared with the WT corneal epithelium. Immunohistochemistry and real-time PCR analysis revealed a significantly decreased expression of corneal epithelial differentiation markers such as K12, Cx43, Notch1, and Pax6 in *Hspg2*$^{-/-}$-Tg mice, compared with those of the WT mice.

Conclusions. The findings of this study highlight a strong correlation between the presence of perlecan in the basement membrane and the structure of corneal epithelium and that the perlecan-deficient mutation impairs corneal epithelial structure. (*Invest Ophthalmol Vis Sci.* 2012;53:1277–1284) DOI:10.1167/iovs.11-8742

The surface of a mammalian cornea is composed of a nonkeratinized, self-renewing, pluristratified epithelium of ectodermal origin. The corneal epithelium consists of basal, wing, and superficial cells that are separated from the stroma by the basement membrane (BM). Corneal epithelial cells exhibit a dynamic homeostasis, turning over approximately every 7 to 10 days. Many cellular processes, such as proliferation, apoptosis, differentiation, migration, adhesion, and stratification, are essential for the structure of corneal epithelium.

Perlecan (Hspg2) is a large (>400 kDa), multidomain heparan sulfate proteoglycan (Hspg) expressed in BM.[1–6] The protein core consists of five domains that share homology with other molecules involved in nutrient metabolism, cell proliferation, and adhesion, including laminin, the low-density lipoprotein (LDL) receptor, epithelial growth factor (EGF), and the neural cell adhesion molecule (N-CAM).[1–3] Within the protein core there are numerous sites for O-linked glycosylation, as well as four potential sites for heparan sulfate (HS)/chondroitin sulfate (CS) chain attachment. These chains, which are usually HS, have been shown to be involved in many interactions, including those associated with growth factors, extracellular matrix (ECM) molecules, and neuromuscular junction proteins.[1–3,7] Perlecan regulates cells through a basic mechanism involving the binding of various proteins via the protein core and/or the glycosaminoglycan chains. In vertebrates, perlecan functions in a diverse range of developmental and biological processes, from the development of cartilage to the regulation of wound healing.[8–13] Recent reports from other groups also emphasized a key role for perlecan in regulating cell proliferation and cell survival in different tissues. For example, it has been reported that perlecan HS deficiency induces apoptosis of lens epithelial cells.[14] Sher et al.[15] found that perlecan regulates both the survival and terminal differentiation steps of keratinocytes and that it is critical for the formation of normal epidermis.

In the cornea, perlecan is expressed in the BM of the corneal epithelium.[16] However, the functions or roles of perlecan in the cornea have yet to be well investigated. Therefore, in the present study, the role of perlecan in the structure of corneal epithelium was investigated by use of perlecan-deficient (*Hspg2*$^{-/-}$-Tg) mice. By genetically disrupting perlecan expression in the BM of corneal epithelium, the results of this study revealed that perlecan is essential in the structure of corneal epithelium. To the best of our knowledge, this study is the first to demonstrate the involvement of perlecan in the structure of the corneal epithelium.

Materials and Methods

Animal Experiments

Some perlecan-deficient (*Hspg2*$^{-/-}$) mice die around embryonic day (E)10 due to defects in the myocardial basement membranes, and the mice that survive this stage die perinatally of premature cartilage development.[12,17] In a previous study, a perlecan transgenic mouse line (Tg, *Col2a1-Hspg2*$^{Tg/-}$) that expresses recombinant perlecan in cartilage was created by use of a cartilage-specific *Col2a1* promoter/enhancer to reverse the cartilage abnormalities of *Hspg2*$^{-/-}$ mice.[13] Perinatal lethality–rescued mice (*Hspg2*$^{-/-}$-Tg, *Hspg2*$^{-/-}$; *Col2a1-*

From the Departments of [1]Ophthalmology and [3]Neurology and the [2]Research Institute for Disease of Old Age, Juntendo University School of Medicine, Tokyo, Japan.

Submitted for publication October 5, 2011; revised November 16, 2011, and January 6, 2012; accepted January 10, 2012.

Disclosure: **T. Inomata**, None; **N. Ebihara** , None; **T. Funaki** , None; **A. Matsuda**, None; **Y. Watanabe**, None; **L. Ning**, None; **Z. Xu**, None; **A. Murakami**, None; **E. Arikawa-Hirasawa**, None

Corresponding author: Nobuyuki Ebihara, Department of Ophthalmology, Juntendo University School of Medicine, 2-1-1 Hongo, Bunkyo-ku, Tokyo 113-8421 Japan; ebihara@juntendo.ac.jp.

TABLE 1. Primary Antibodies

Antigen	Class	Dilution	Supplier
Anti-perlecan	Rabbit polyclonal	1/100	Seigaku, Tokyo Japan
Anti-Ki67	Rabbit polyclonal	1/200	Abcam, Cambridge UK
Anti-cytokeratin12	Goat polyclonal	1/200	Santa Cruz Biotech, Santa Cruz, CA
Anti-connexin43	Rabbit polyclonal	1/2000	Abcam
Anti-Notch1	Rabbit polyclonal	1/200	Abcam
Anti-Pax6	Mouse monoclonal	1/200	R&D Systems Minneapolis, MN

Hspg$^{+/Tg}$) were then created by mating the transgenic mice with heterozygous *Hspg2*$^{+/-}$ mice. The *Hspg2*$^{-/-}$-Tg mice exhibited normal cephalic development, and those mice were then maintained in a mixed genetic background of C57BL/6 and SVJ 129. In this study, we used 8- and 16-week-old *Hspg2*$^{-/-}$-Tg mice and *Hspg2*$^{+/+}$-Tg mice as well as wild-type (WT) mice, and the eyes of those mice were dissected and prepared for histologic or molecular analysis. All animal experiments in this study were performed in accordance with the guidelines set forth in the ARVO Statement for the Use of Animals in Ophthalmic and Vision Research.

Histologic Analysis

The excised mouse eyes were fixed in 20% formalin in phosphate-buffered saline (PBS) at 4°C overnight and then embedded in paraffin. Next, 3-μm-thick sections of the eyes were mounted on microslides (New Silane; Muto-Glass, Tokyo, Japan). Histologic examination was performed after Harris hematoxylin and eosin (H-E) staining. Histology of the corneas of the 8-week-old *Hspg2*$^{-/-}$-Tg and WT mice littermates was then compared by use of light microscopy (AX80; Olympus Corp., Tokyo, Japan).

Morphometric Measurements

For the morphometric measurements, corneal thicknesses were calculated in 8-week-old *Hspg2*$^{-/-}$-Tg and WT mice. Next, 3-μm-thick tissue sections of the cornea stained with H-E staining were viewed by light microscopy (40× magnification) with a computerized image analyzer (KS400; Carl Zeiss AG, Oberkochen, Germany), and measurements were made by use of a calibrated eyepiece graticule. Corneal thickness was measured in the central region of the serial sections of each eye. The mean thickness was then calculated by averaging those measurements. The epithelial, stromal, endothelial, and whole corneal thicknesses were then compared. The ratio of the epithelial cell layer thickness to the full corneal thickness was also calculated.

Examination by Transmission Electron Microscopy

For the transmission electron microscopy (TEM) examinations, the eyes of 8- and 16-week-old *Hspg2*$^{-/-}$-Tg and WT mice were dissected and fixed in cold 2.5% glutaraldehyde with PBS overnight at 4°C and then sectioned into small pieces. Those sections were then postfixed with 2% osmium tetroxide in the same buffer, dehydrated through a series of ethyl alcohol solutions, and embedded in Epon. All sections were examined by use of an electron microscope (H-7100; Hitachi, Tokyo, Japan) at an accelerating voltage of 75 kV.

Immunohistochemical Staining

Deparaffinized sections were washed in 100% ethanol and rehydrated with PBS. Antigen retrieval was performed by boiling the sections in 0.01 M citrate buffer (pH 6) for 10 minutes. Next, the slides were washed with PBS and blocked with 4% normal serum (species selected according to the secondary antibody) in PBS and 0.3% bovine serum albumin for 10 minutes at room temperature. The slides were incubated with primary antibody overnight at 4°C (Table 1), washed with PBS, incubated with the secondary antibodies, and counterstained with DAPI (H-1200; Vector Laboratories, Inc., Burlingame, CA). Ki67-positive cells were quantified by capturing the image of individual nuclei from *Hspg2*$^{-/-}$-Tg and WT sections processed in parallel and immunostained on the same slides. All sections were viewed with a fluorescence microscope (AxioVision 3.1; Carl Zeiss Meditec, Inc.) and confocal microscopy (TCS-SP5/TIRF; Leica Microsystems AG, Solms, Germany).

Assessment of Cell Death by TUNEL Assay

Deparaffinized sections were rehydrated through graded alcohols and then washed with PBS. The tissue sections were treated with proteinase K (80 μg/mL) for 20 minutes at room temperature. The slides were then washed twice with PBS. Next, the TUNEL assay (TUNEL in Situ Cell Death Detection Kit, fluorescein; Roche Diagnostics GmbH, Mannheim, Germany) was performed according to the manufacturer's instructions. Briefly, the sections were first counterstained with DAPI. The samples were then visualized by fluorescence microscopy, and images were obtained for quantitative analysis. TUNEL-positive cells were then quantified by capturing the image of individual nuclei from *Hspg2*$^{-/-}$-Tg and WT sections processed in parallel and immunostained on the same slides.

TABLE 2. Primers Used in RT-PCR

Gene	Primer	Primer Sequence
Ki67	Forward	5′-GCAGGAAGCAACAGATGAGAAGCC-3′
	Reverse	5′-GCTCAGGTGATACATGCCTCCTGC-3′
Active caspase3	Forward	5′-AGGTGGCAACGGAATTCGAGTC-3′
	Reverse	5′-ACACGGGATCTGTTTCTTTGCG-3′
Cytokeratin12	Forward	5′-TCTTCATGCTGGTGGTGTCCTTG-3′
	Reverse	5′-TCAAGAAACCAGGCCTCTGCATC-3′
Connexin43	Forward	5′-TCTTCATGCTGGTGGTGTCCTTG-3′
	Reverse	5′-CGATCCTTAACGCCCTTGAAGAAG-3′
Notch1	Forward	5′-GGAGGACCTCATCAACTCACATGC-3′
	Reverse	5′-CCGTTCTTCAGGAGCACAACAG-3′
Pax6	Forward	5′-AAGGATGTTGAACGGGCAGAC-3′
	Reverse	5′-TGTTGCTGGCAGCCATCTTG-3′
GAPDH	Forward	5′-AAGAGAGGCCCTATCCCAACTC-3′
	Reverse	5′-TTGTGGGTGCAGCGAACTTTATTG-3′

Analysis by Real-Time Polymerase Chain Reaction

Total RNA was isolated from the dissected corneas (NucleoSpin RNA II; Macherey-Nagel GmbH, KG, Duren, Germany) according to the manufacturer's instructions. cDNA was generated from 1.0 μg total RNA (ReverTra Ace-α; Toyobo Co., Ltd., Osaka, Japan). Real-time PCR was performed with SYBR green master mix (Fast SYBR Green Master Mix; Applied Biosystems, Inc. [ABI], Foster City, CA) on a commercial system (Prism 7500; ABI). In this study, we did not isolate the RNA from the epithelia but from the whole cornea. Therefore, the PCR analysis for the level of reduced expression of differentiation and developmental regulator molecules in *Hspg2*$^{-/-}$-Tg eyes may be semiquantitative, not absolutely quantitative. Primers sequences are listed in Table 2.

Results

Histologic Analysis of the *Hspg2*$^{-/-}$-Tg Eyes

The eyes of 8-week-old *Hspg2*$^{-/-}$-Tg mice that were approximately the same body weight and length as WT mice exhibited microphthalmos and a small palpebral fissure (Fig. 1A). Under light microscopy at low magnification, the *Hspg2*$^{-/-}$-Tg eyes stained with H-E staining also exhibited microphthalmos (Figs. 1B, 1C). Under high magnification, the *Hspg2*$^{-/-}$-Tg eyes showed a thinner corneal epithelium compared with that of the WT eyes (Figs. 1D, 1E). The localization of perlecan was examined by immunostaining with specific antibody for their core protein. Eight-week-old WT and *Hspg2*$^{-/-}$-Tg mice were stained with anti-perlecan antibody (Alexa488, green), and the corneal nuclei were stained with DAPI (blue). Perlecan was strongly expressed in the corneal epithelial BM of the WT mice (Fig. 1F). However, the expression of perlecan was not recognized in the corneal epithelium of the *Hspg2*$^{-/-}$-Tg mice (Fig. 1G).

Analysis by TEM

TEM was performed to further examine the corneal morphology in the *Hspg2*$^{-/-}$-Tg and WT mice. The corneal epithelia from WT mice and *Hspg2*$^{-/-}$-Tg, 8 weeks (Figs. 2A, 2B) and 16 weeks (Figs. 2C, 2D) of age, were analyzed by TEM. At 8 and 16 weeks of age, the *Hspg2*$^{-/-}$-Tg mice showed thinner corneal epithelia compared with the WT mice. Eight-week-old WT mice showed 9 to 10 corneal epithelial layers (Fig. 2A). In contrast, the 8-week-old *Hspg2*$^{-/-}$-Tg mice showed thinner undifferentiated wing cell layers compared with the WT mice (Fig. 2B). Corneal wing-cell layers of the 16-week-old *Hspg2*$^{-/-}$-Tg mice were thinner and undifferentiated compared with those of the WT mice. As the ages of the mice progressed, the *Hspg2*$^{-/-}$-Tg mice showed a thinner corneal epithelium compared with that of the WT mice (Fig. 2A-D). Under high magnification, no significant difference was observed between the *Hspg 2*$^{-/-}$ Tg mice and WT mice in regard to the structure of superficial cells (Figs. 2E, 2F), basal cells (Figs. 2G, 2H), and epithelial BM (Figs. 2I, 2J).

In the corneal stromal layer, the keratocytes were localized between stromal lamellae, with no significant difference found between the 8-week-old *Hspg2*$^{-/-}$-Tg and WT mice (Figs. 3A, 3B). Under high magnification, cross-sections of the collagen fibers from the *Hspg2*$^{-/-}$-Tg and WT mice demonstrated parallel bundles of a regular diameter (Figs. 3C, 3D). Under low magnification, no significant difference was observed between the *Hspg2*$^{-/-}$-Tg and WT mice as to the thickness of the endothelial layers (Figs. 3E, 3F). Under high magnification, Descemet's membrane was found to be composed of electron-dense material in both the *Hspg2*$^{-/-}$-Tg and WT mice (Figs. 3G, 3H). The corneal endothelium was found to have some desmosomes and gap junctions, with no significant difference found between the *Hspg2*$^{-/-}$-Tg and WT mice (Figs. 3I, J).

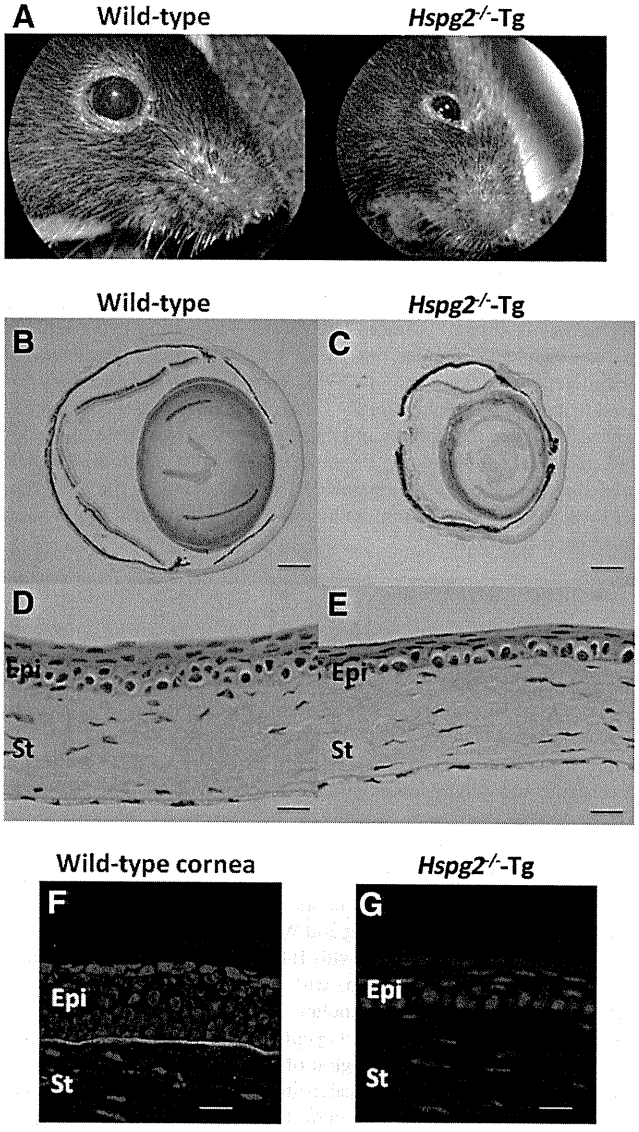

Figure 1. Histologic analysis. Representative macroscopic images of the eye in situ (**A**). H-E-stained sections (**B–E**) show the histologic features of whole eyes visualized by light microscopy at low (**B**, **C**) and high (**D**, **E**) magnifications. The 8-week-old *Hspg2*$^{-/-}$-Tg mice had microphthalmos, whereas the WT mice did not (**A–C**). The corneal epithelium of the 8-week-old *Hspg2*$^{-/-}$-Tg mice thinner than that of the WT mice (**D**, **E**). Immunohistochemical staining of perlecan in the corneas of the WT and the *Hspg2*$^{-/-}$-Tg mice (**F**, **G**). Perlecan (Alexa 488, *green*) was strongly expressed in the corneal epithelial basement membrane of the WT mice (**F**). However, the expression of perlecan was not recognized in the corneal epithelium of the *Hspg2*$^{-/-}$-Tg mice (**G**). Epi, epithelium; St, stroma. Scale bars: (**B**, **C**) 600 μm; (**D**, **E**) 40 μm; (**F**, **G**) 30 μm.

Corneal Thickness Morphometry

The thickness of the corneal epithelium was examined in the 8-week-old mice, as that is the age at which the development of the corneal epithelium is complete. Histologic examination of those mice revealed that the corneal epithelial thickness was markedly thinned in the *Hspg2*$^{-/-}$-Tg mice. The corneal thickness of the central region was then calculated (Fig. 4A). The thickness of the central whole corneal cell layers was found to

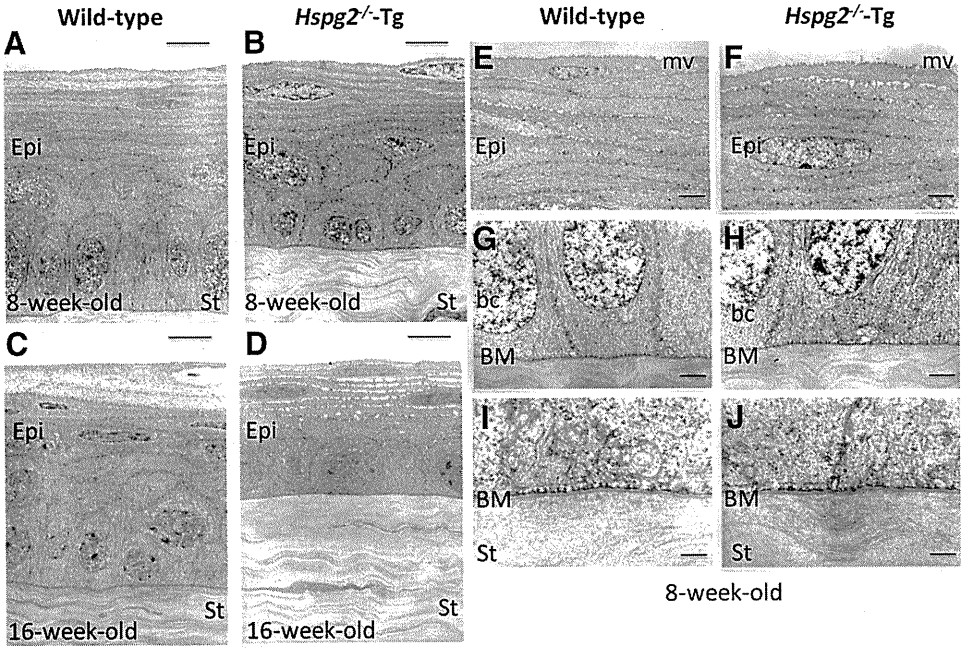

FIGURE 2. TEM of the corneal epithelium. TEM images show ultrastructural features of corneal epithelium from WT (A, C, E, G, I) and $Hspg2^{-/-}$-Tg (B, D, F, H, J) mice. Corneal epithelia of the 8- and 16-week-old $Hspg2^{-/-}$-Tg mice (B, D) were thinner and had thinner wing cell layers compared with those of the WT mice (A, C). As the ages of the mice progressed, the corneal epithelium of the 16-week-old $Hspg2^{-/-}$-Tg mice became thinner and the wing cell layer was undifferentiated compared with that of the WT mice (D). Under high magnification, no significant difference was observed between the $Hspg2^{-/-}$-Tg mice and WT mice in regard to the structure of the superficial cells (E, F), basal cells (G, H), and epithelial basement membrane (I, J). Epi, epithelium; St, stroma; mv, microvilli; bc, basal cell, BM, corneal basement membrane. Scale bar: (A–D) 5 μm; (E-H) 2 μm; (I, J) 0.5 μm.

be 25.6% thinner in the $Hspg2^{-/-}$-Tg mice (on average, 85.12 μm thick compared with 114.53 μm in the WT mice; $n = 6$; $P = 0.0411$). The thickness of the central epithelial cell layers was found to be 45.5% thinner in the $Hspg2^{-/-}$-Tg mice (on average, 18.51 μm thick compared with 33.94 μm in the WT mice; $n = 6$; $P = 0.0022$). The average thicknesses of the central corneal stromal layers and endothelial layers were not significantly different between the $Hspg2^{-/-}$-Tg and WT mice. Because of the microphthalmos of the eyes of the $Hspg2^{-/-}$-Tg mice, we calculated the comparison of the ratio of the epithelial cell layer thickness to the full central corneal thickness in the central region (Fig. 4B). The ratio of the central epithelial cell layer thickness to the central whole corneal thickness was found to be significant lower in the $Hspg2^{-/-}$-Tg mice, 22.6% compared with 29.4% in the WT mice ($n = 6$, $P = 0.0043$). These findings suggest that the corneal epithelial cell layer in the $Hspg2^{-/-}$-Tg mouse is thinner regardless of the microphthalmos.

Proliferation and Cell Death in $Hspg2^{-/-}$-Tg Corneal Epithelium

We posited that the findings of thinner corneal epithelium in the 8-week-old $Hspg2^{-/-}$-Tg mice could be the result of a decrease in cell proliferation or an increase in cell death. To discern between these two possibilities, immunostaining was performed to investigate the number of Ki67-positive (Figs. 5A1, A2) and TUNEL-positive (Figs. 5D1, 5D2) cells. The Ki67 antigen was designated as a marker for cell proliferation, and the number of Ki67-positive cells was scored across the entire section of the corneal epithelium. The average ratio of Ki67-positive cells to basal cells was 12% per section in the $Hspg2^{-/-}$-Tg epithelium, compared with 21% in the WT epithelium ($n = 6$; $P = 0.0087$; Fig. 5B). Real-time PCR for Ki67 showed a 67% decrease in RNA levels in the $Hspg2^{-/-}$-Tg epithelium ($n = 5$; $P = 0.0159$; Fig. 5C).

TUNEL assay assessment of cell death revealed a very small number of TUNEL-positive cells (<0.3%) per corneal section in

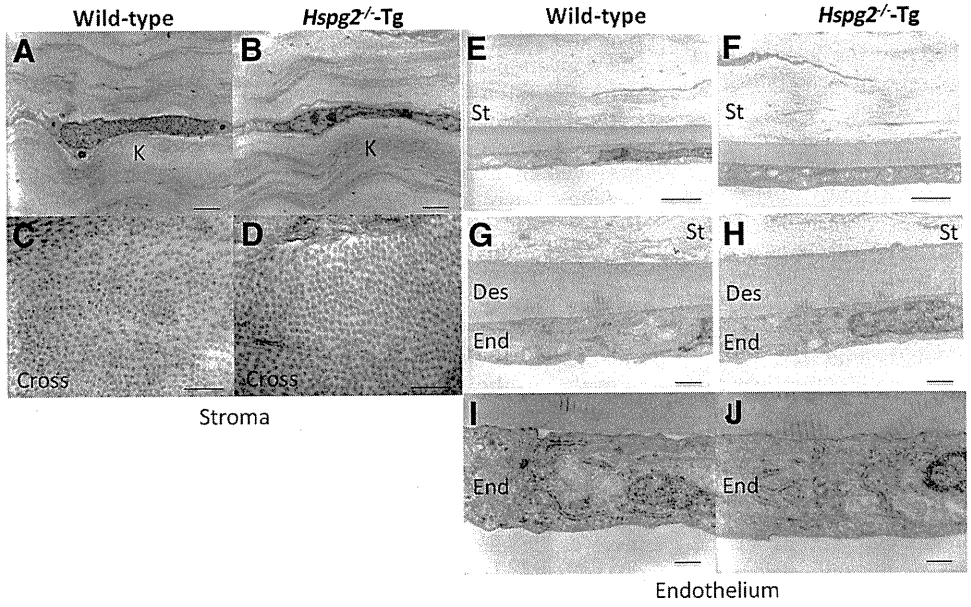

FIGURE 3. Electron microscopy of corneal stroma and endothelium. Keratocytes (A, B). Collagen fibers cut in cross-section (C, D). Stroma and corneal endothelium observed under low magnification (E, F). Descemet's membrane observed under high magnification (G, H). Corneal endothelium observed under high magnification (I, J). No significant differences were found between the 8-week-old $Hspg2^{-/-}$-Tg mice and WT mice in regard to the construction of the stroma and endothelium. K, keratocytes; St, stroma; Des, Descemet's membrane; End, endothelium. Scale bar: (A, B) 2 μm; (C, D, I, J) 0.5 μm; (E, F) 5 μm; (G, H) 1 μm.

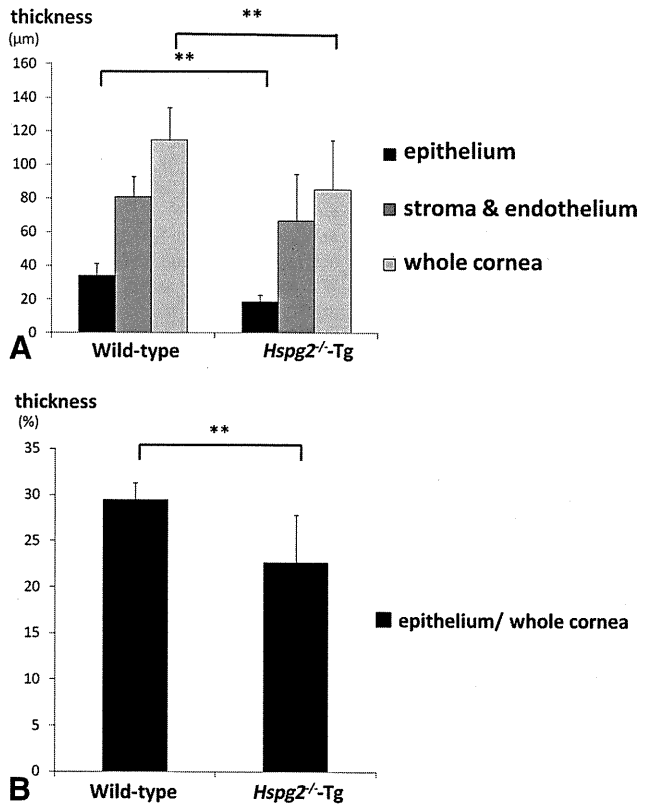

FIGURE 4. Morphometry of corneal thickness. Comparison of central corneal thickness. (**A**) The central corneal epithelial cell layer of the 8-week-old *Hspg2*$^{-/-}$-Tg mice was significantly thinner than that of the 8-week-old WT mice (n = 6; P = 0.0022). The full central corneal thickness was significantly thinner in the 8-week-old *Hspg2*$^{-/-}$-Tg mice compared with that in the 8-week-old WT mice (n = 6; P = 0.0411). Comparison of the ratio of the epithelial cell layer thickness to the full corneal thickness measured at the central cornea (**B**). The ratio of epithelial cell layer thickness to full corneal thickness was significantly lower in the *Hspg2*$^{-/-}$-Tg mice than in the WT mice (n = 6; P = 0.0043; Mann-Whitney U test: *P < 0.05, **P < 0.01, ***P < 0.0001).

both the *Hspg2*$^{-/-}$-Tg and WT epithelium (Fig. 5E), and there was no increase in RNA levels of active caspase3 of the apoptosis marker in both *Hspg2*$^{-/-}$-Tg and WT corneal epithelium (Fig. 5F), thus indicating that the loss of perlecan did not lead to a significant change in the rate of apoptosis. Therefore, the likely cause of the thinning of the 8-week-old *Hspg2*$^{-/-}$-Tg corneal epithelium was determined to be reduced cell proliferation.

Effect of Perlecan Deficiency on the Expression of Markers of Corneal Epithelial Differentiation

The expression of cytokeratin12 (K12), a corneal differentiation marker, in the 8-week-old *Hspg2*$^{-/-}$-Tg mice was significantly decreased compared with that in the WT mice examined by immunohistochemistry (Figs. 6A1, A2). Real-time PCR for K12 in the *Hspg2*$^{-/-}$-Tg epithelium showed a 54% decrease in RNA levels compared with the WT epithelium (n = 5; P = 0.4698; Fig. 6E). Connexin43 (Cx43), a gap junction protein, was found to be present in the corneal basal cell layers in the WT epithelium, but was absent in the *Hspg2*$^{-/-}$-Tg epithelium by immunohistochemistry (Figs. 6B1, 6B2). Real-time PCR for Cx43 in the *Hspg2*$^{-/-}$-Tg epithelium showed a 41% decrease in RNA levels compared with that in the WT epithelium (n = 5; P = 0.4698; Fig. 6E). The expression of Notch1 in the *Hspg2*$^{-/-}$-Tg corneal epithelium was significantly decreased compared with that of the WT epithelium by immunohistochemistry (Figs. 6C1, 6C2). Real-time PCR showed that the *Hspg2*$^{-/-}$-Tg mutation caused a significantly decrease in Notch1 RNA levels in the corneal epithelium, compared with that in the WT mice (n = 5; P = 0.0159; Fig. 6E). The expression of Pax6, a developmental regulator marker, was shown by immunohistochemistry to be significantly decreased in the corneal epithelium in the *Hspg2*$^{-/-}$-Tg mice compared with that of the WT mice (Figs. 6D1, 6D2). Real-time PCR for Pax6 in the *Hspg2*$^{-/-}$-Tg epithelium showed a significant decrease in RNA levels compared with that in the WT epithelium (n = 5; P = 0.0159; Fig. 6E).

DISCUSSION

In this study, perlecan was identified in corneal epithelial BM and the epithelium was shown to be thin and poorly differentiated in perlecan-deficient mice (*Hspg2*$^{-/-}$-Tg) and accompanied by the downregulation of Ki67, K12, Cx43, Notch1, and Pax6. However, the gross morphology of the corneal epithelium was not retarded in the *Hspg2*$^{-/-}$-Tg mice, suggesting that perlecan is not critically necessary in this process. Therefore, perlecan may be essential for the structure but not the development of corneal epithelium. In normal corneal epithelium, epithelial cells in the last phase of their differentiation undergo apoptosis as they reach the superficial cell layer. Since the cell death rate of the corneal epithelial cells in the *Hspg2*$^{-/-}$-Tg mice was similar to that in WT mice, the failure of those cells to form multilayered corneal epithelium must be due to the apparent decrease in the proliferation and differentiation rates in corneal epithelial cells. In this present study, we revealed that the expression of Ki67, K12, Cx43, Notch 1, and Pax6, which are markers of cell proliferation and differentiation, was reduced in the *Hspg2*$^{-/-}$-Tg mice, compared with that of the WT mice. Therefore, our findings revealed that perlecan in the BM of corneal epithelium may be critical for normal epithelial formation and terminal differentiation.

It has been reported that K12 is essential for the differentiation and maintenance of corneal epithelium integrity.,[18,19] Targeted deletion of K12 in a mouse model showed fewer cellular layers in the corneal epithelium and corneal fragility.[19] The findings of this study showed that downregulation of the expression of K12 at protein and RNA levels may be one of the causes of aberrant differentiation in the *Hspg2*$^{-/-}$-Tg corneal epithelium. From another aspect, it has been reported that the gap junction marker Cx43 mediates the intercellular diffusion ions and other small molecules,[20-22] thereby contributing to the regulation of tissue differentiation and homeostasis.[23] Of particular interest, the expression of Cx43 was noted in the corneal epithelial basal cells in the WT corneal epithelium, but not in the *Hspg2*$^{-/-}$-Tg epithelium, thus suggesting that the basal cell environment is impaired by gap junction functional decline. Therefore, the downregulation of Cx43 in the *Hspg2*$^{-/-}$-Tg mice most likely impairs the differentiation and structure of the corneal epithelium.

It has been reported that the Notch signaling pathway, another corneal homeostasis marker, limits cell proliferation and promotes differentiation.[24-27] In this study, the expression of Notch1 was decreased in the *Hspg2*$^{-/-}$-Tg mice, compared with that in the WT mice. Recently, Vauclair et al.[27] demonstrated that Notch1-deficient corneal cells lose their ability to heal and repair wounded corneal epithelium. The findings of that study showed that instead of generating new corneal epithelium after injury, those cells repair the wound by forming a hyperproliferative epidermislike epithelium. This process involves the secretion of FGF-2 through Notch1 signaling in the epithelium.[27] It is well known that FGF-2 is a growth factor of corneal epithelial cells.[28,29] Loss of Notch 1 in the corneal

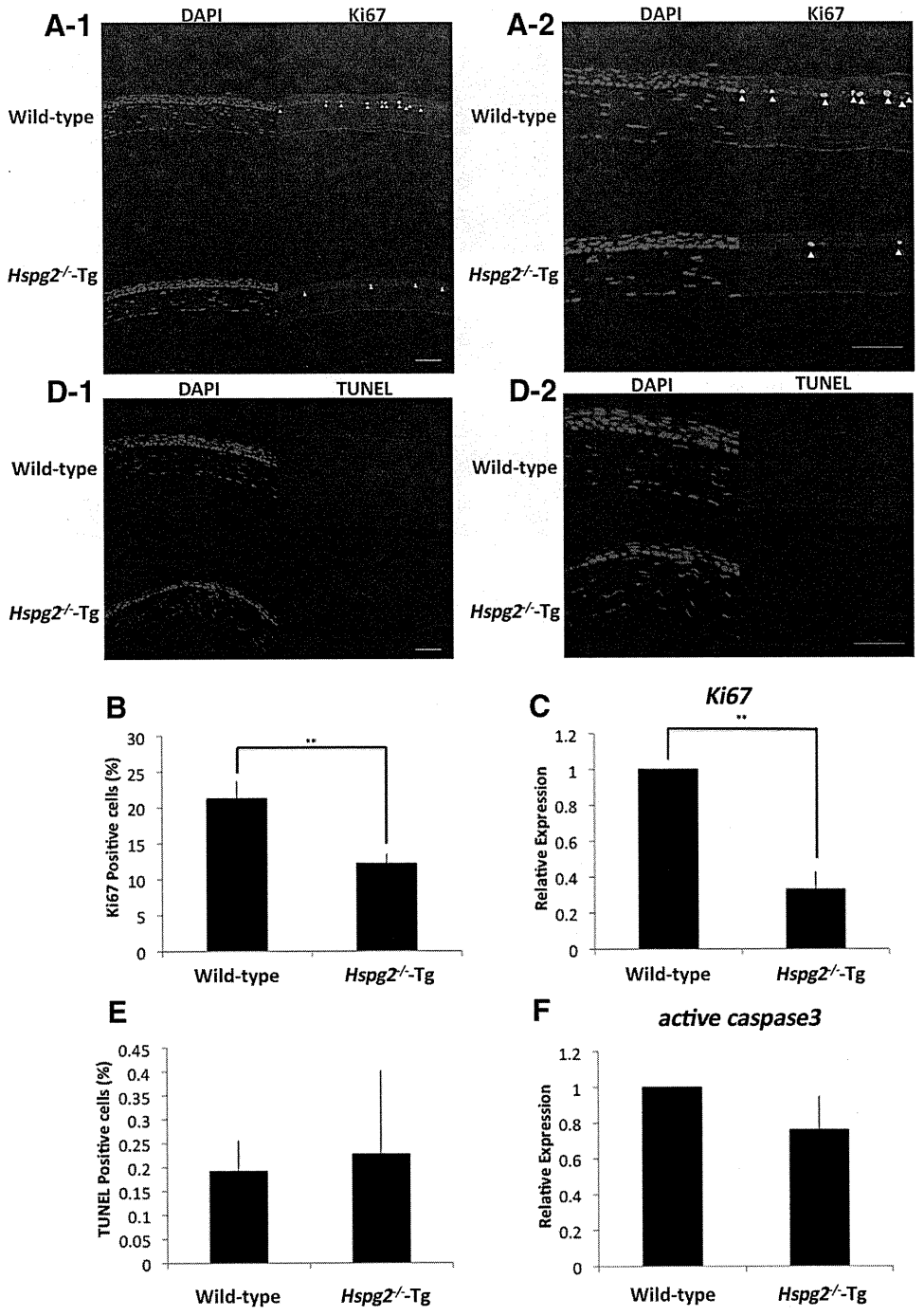

FIGURE 5. Proliferation and cell death in the *Hspg2*$^{-/-}$-Tg corneal epithelium. Immunohistochemistry showed a decreased number of cells containing Ki67 (Alexa488, *green*, *white arrow*) in the 8-week-old *Hspg2*$^{-/-}$-Tg versus WT corneal epithelium (DAPI, *blue*; **A1**, **A2**). The percentage of Ki67-positive cells in the corneal epithelium showed a 9.0% decrease in the *Hspg2*$^{-/-}$-Tg mice (±SEM, $n = 6$, $P = 0.0087$; **B**). Quantification of RNA levels for Ki67 in the corneal epithelium (±SEM; $n = 5$; $P = 0.0159$; **C**). In the superficial corneal cells, there was almost no TUNEL-positive staining (**D1**, **D2**). The percentage of TUNEL-positive cells in the corneal epithelium (±SEM, $n = 6$; **E**). Quantification of RNA levels for active caspase3 in the corneal epithelium (±SEM; $n = 5$; **F**; Mann-Whitney U test: $^{*}P < 0.05$, $^{**}P < 0.01$, $^{***}P < 0.0001$). Scale bar: 50 μm. Low magnification: **A1**, **D1**; high magnification: **A2**, **D2**.

epithelium resulted first in upregulation of FGF-2 by the corneal epithelium, suggesting that Notch1 signaling repressed its expression.[27] Despite the decreased expression of Notch1, a hyperproliferative change of corneal epithelium was not observed in the *Hspg2*$^{-/-}$-Tg mice. Since FGF-2 is a ligand of perlecan, there may be a possibility that a high dose of FGF-2 could not be maintained in the BM of the corneal epithelium of *Hspg2*$^{-/-}$-Tg mice.[30–35] Reportedly, FGF-7 is also a ligand of perlecan.[1] In a recent study, Lovicu et al.[36] showed hyperproliferation of embryonic corneal epithelial cells in transgenic mice engineered to overexpress human FGF-7 in the eye. Chikama et al.[37] analyzed the effects of excess FGF-7 on both the proliferation and differentiation of corneal epithelium in an FGF-7 transgenic mouse model in which cornea-specific FGF-7 was overexpressed. In that study, the mice exhibited epithelial hyperplasia, accompanied by the downregulation of K12. According to these results, the mechanism of the poor differentiation of the epithelium in *Hspg2*$^{-/-}$-Tg mice is due to the lack of the FGF-2 or FGF-7 that links to perlecan in the BM. Therefore, the strong correlation between the presence of perlecan in the BM and the formation of normal corneal epithelium suggests that perlecan functions as a reservoir for soluble factors involved in the proliferation and differentiation of corneal epithelial cells.

It should be noted that the *Hspg2*$^{-/-}$-Tg mice had microphthalmos. This condition has been reported in Pax6-deficient mice.[38–41] These reports suggest that Pax6 is a key developmental regulator and that it is generally essential for morphogenesis in the eye. Pax6 has autonomous roles in all eye tissues, where it is expressed at several developmental stages. Re-

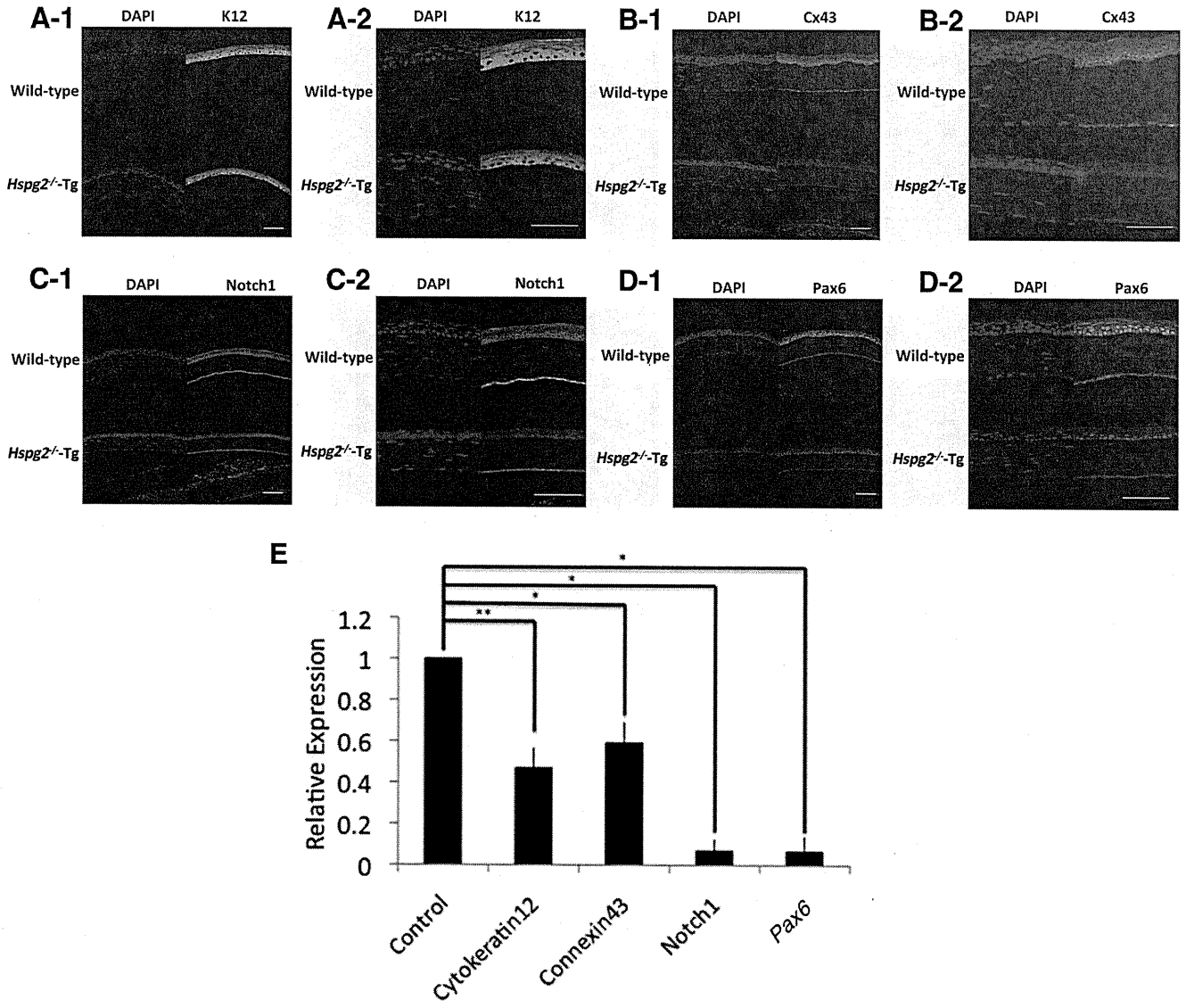

FIGURE 6. Expression of differentiation and developmental regulator markers in the 8-week-old *Hspg2*$^{-/-}$-Tg corneal epithelium demonstrated that the expression of cytokeratin12 (K12) in the *Hspg2*$^{-/-}$-Tg epithelium was significantly decreased compared with that in the WT epithelium (**A1**, **A2**). *Hspg2*$^{-/-}$-Tg corneal epithelium showed no expression of Connexin43 (Cx43; **B1**, **B2**). The expression of Notch1 in *Hspg2*$^{-/-}$-Tg corneal epithelium was significantly decreased compared with that in the WT epithelium (**C1**, **C2**). *Hspg2*$^{-/-}$-Tg corneal epithelium showed decreased Pax6 expression compared with that in the WT epithelium (**D1**, **D2**). Quantification of RNA levels for differentiation and developmental regulator markers in corneal epithelium (±SEM, $n = 5$; **E**; Mann-Whitney U test: $^{*}P < 0.05$, $^{**}P < 0.01$, $^{***}P < 0.0001$). Scale bar: 50 μm. Low magnification: **A1**, **B1**, **C1**, **D1**; high magnification: **A2**, **B2**, **C2**, **D2**.

cently, a report by Garcia-Villegas et al.[42] revealed that Pax6 is the earlier differentiation marker expressed by corneal epithelial cells and that it is the main driver of the differentiation of corneal epithelial cells, as the expression of Pax6 promotes the differentiation of corneal epithelial cells. On the other hand, transgenic mice overexpressing Pax6 in the corneal epithelium also showed abnormal epithelial cell morphology. These results indicate that a correct Pax6 dosage for the normal development of corneal epithelium may be important. In this present study, we demonstrated that the corneal epithelium of *Hspg2*$^{-/-}$-Tg mice was thinner and not well differentiated and that the phenotypes became more severe with age. The corneal epithelial phenotype was similar to that of Pax6-deficient mice. Thus, the downregulation of Pax6 in the corneal epithelium of *Hspg2*$^{-/-}$-Tg mice is likely to be a factor in the observed microphthalmos and thinner epithelium. We theorize that the downregulation of K12, Cx43, Notch1, and Pax6 probably occurs to prevent the proliferation and the differentiation from basal cells to wing cells, thus making the corneal epithelium of *Hspg2*$^{-/-}$-Tg mice thinner than that of WT mice with downregulation of the expression of Ki67.

In summary, by using perlecan-deficient mice (*Hspg2*$^{-/-}$-Tg) we demonstrated for the first time that perlecan is essential for the structure of corneal epithelium, as it controls the expression of markers for the proliferation or differentiation of corneal epithelial cells. Our findings revealed that perlecan in the BM of corneal epithelium were critical for normal epithelial structure and terminal differentiation.

Acknowledgments

The authors thank Glenn Longenecker and Ashok B. Kulkarni for help in creating the mutant mice, Yoshihiko Yamada for critical reading of the manuscript, and Saori Ito for secretarial assistance.

References

1. Knox SM, Whitelock JM. Perlecan: how does one molecule do so many things? *Cell Mol Life Sci.* 2006;63:2435-2445.
2. Murdoch AD, Dodge GR, Cohen I, Tuan RS, Iozzo RV. Primary structure of the human heparin sulfate proteoglycan from basement membrane (HSPG2/perlecan): a chimeric molecule with multiple domains homologous to the low density lipoprotein receptor, laminin, neural cell adhesion molecules, and epidermal growth factor. *J Biol Chem.* 1992;267:8544-8557.
3. Noonan DM, Fulle A, Valente P, et al. The complete sequence of perlecan, a basement membrane heparan sulfate proteoglycan, reveals extensive similarity with laminin A chain, low density lipoprotein-receptor, and the neural cell adhesion molecule. *J Biol Chem.* 1991;26:22939-22947.
4. Hassell JR, Robey PG, Barrach HJ, et al. Isolation of a heparan sulfate-containing proteoglycan from basement membrane. *Proc Natl Acad Sci USA.* 1980;77:4494-4498.
5. Iozzo RV. Perlecan: a gem of a proteoglycan. *Matrix Biol.* 1994; 14:203-208.
6. Iozzo RV. Basement membrane proteoglycans: from cellar to ceiling. *Nat Rev Mol Cell Biol.* 2005;6:646-656.
7. Whitelock JM, Iozzo RV. Heparan sulfate: a complex polymer charged with biological activity. *Chem Rev.* 2005;105:2745-2764.
8. Handler M, Yurchenco PD, Iozzo RV. Developmental expression of perlecan during murine embryogenesis. *Dev Dyn.* 1997;210:130-145.
9. Knox S, Melrose J, Whitelock J. Electrophoretic, biosensor, and bioactivity analyses of perlecans of different cellular origins. *Proteomics.* 2001;1:1534-1541.
10. Jiang X, Couchman JR. Perlecan and tumor angiogenesis. *J Histochem Cytochem.* 2003;51:1393-1410.
11. Zhou Z, Wang J, Cao R, et al. Impaired angiogenesis, delayed wound healing and retarded tumor growth in perlecan heparan sulfate-deficient mice. *Cancer Res.* 2004;64:4699-4702.
12. Arikawa-Hirasawa E, Watanabe H, Takami H, Hassell JR, Yamada Y. Perlecan is essential for cartilage and cephalic development. *Nat Genet.* 1999;23:354-358.
13. Xu Z, Ichikawa N, Kosaki K, et al. Perlecan deficiency causes muscle hypertrophy, a decrease in myostatin expression, and changes in muscle fiber composition. *Matrix Biol.* 2010;29:461-470.
14. Rossi M, Morita H, Sormunen R, et al. Heparan sulfate chains of perlecan are indispensable in the lens capsule but not in the kidney. *EMBO J.* 2003;22:236-245.
15. Sher I, Zisman-Rozen S, Eliahu L, et al. Targeting perlecan in human keratinocytes reveals novel roles for perlecan in epidermal formation. *J Biol Chem.* 2006;281:5178-5187.
16. Kabosova A, Azar DT, Bannikov GA, et al. Compositional differences between infant and adult human corneal basement membranes. *Invest Ophthalmol Vis Sci.* 2007;48:4989-4999.
17. Costell M, Gustafsson E, Aszódi A, et al. Perlecan maintains the integrity of cartilage and some basement membranes. *J Cell Biol.* 1999;147:1109-1122.
18. Chaloin-Dufau C, Sun TT, Dhouailly D. Appearance of the keratin pair K3/K12 during embryonic and adult corneal epithelial differentiation in the chick and in the rabbit. *Cell Differ Dev.* 1990;32: 97-108.
19. Kao WW, Liu CY, Converse RL, et al. Keratin 12-deficient mice have fragile corneal epithelia. *Invest Ophthalmol Vis Sci.* 1996;37: 2572-2584.
20. Kimura K, Teranishi S, Nishida T. Establishment of human corneal epithelial cells stably expressing human connexin43. *Exp Eye Res.* 2010;90:4-9.
21. Ko JA, Yanai R, Morishige N, Takezawa T, Nishida T. Upregulation of connexin43 expression in corneal fibroblasts by corneal epithelial cells. *Invest Ophthalmol Vis Sci.* 2009;50:2054-2060.
22. Yang HS, Lu XH, Chen DY, et al. Upregulated expression of connexin43 in spinal ligament fibroblasts derived from patients presenting ossification of the posterior longitudinal ligament. *Spine* (Phila Pa 1976). 2011;36:2267-74.
23. Kumar NM, Gilula NB. The gap junction communication channel. *Cell.* 1996;84:381-388.
24. Ma A, Boulton M, Zhao B, Connon C, Cai J, Albon J. A role for notch signaling in human corneal epithelial cell differentiation and proliferation. *Invest Ophthalmol Vis Sci.* 2007;48:3576-3585.
25. Djalilian AR, Namavari A, Ito A, et al. Down-regulation of Notch signaling during corneal epithelial proliferation. *Mol Vis.* 2008;14: 1041-1049.
26. Thomas PB, Liu YH, Zhuang FF, et al. Identification of Notch-1 expression in the limbal basal epithelium. *Mol Vis.* 2007;13:337-344.
27. Vauclair S, Majo F, Durham AD, et al. Corneal epithelial cell fate is maintained during repair by Notch1 signaling via the regulation of vitamin A metabolism. *Dev Cell.* 2007;13:242-253.
28. Hu C, Ding Y, Chen J, et al. Basic fibroblast growth factor stimulates epithelial cell growth and epithelial wound healing in canine corneas. *Vet Ophthalmol.* 2009;12:170-175.
29. Wang X, Zhou X, Ma J, et al. Effects of keratinocyte growth factor-2 on corneal epithelial wound healing in a rabbit model of carbon dioxide laser injury. *Biol Pharm Bull.* 2010;33:971-976.
30. Friesel RE, Maciag T. Molecular mechanisms of angiogenesis: fibroblast growth factor signal transduction. *FASEB J.* 1995;9:919-925.
31. Takehara K. Growth regulation of skin fibroblasts. *J Dermatol Sci.* 2000;24(suppl 1):S70-S77.
32. Aviezer D, Hecht D, Safran M, et al. Perlecan, basal lamina proteoglycan, promotes basic fibroblast growth factor-receptor binding, mitogenesis, and angiogenesis. *Cell.* 1994;79:1005-1013.
33. Knox S, Merry C, Stringer S, Melrose J, Whitelock J. Not all perlecans are created equal: interactions with fibroblast growth factor (FGF) 2 and FGF receptors. *J Biol Chem.* 2002;277:14657-14665.
34. Whitelock JM, Murdoch AD, Iozzo RV, Underwood PA. The degradation of human endothelial cell-derived perlecan and release of bound basic fibroblast growth factor by stromelysin, collagenase, plasmin, and heparanases. *J Biol Chem.* 1996;271:10079-10086.
35. Whitelock JM, Graham LD, Melrose J, et al. Human perlecan immunopurified from different endothelial cell sources has different adhesive properties for vascular cells. *Matrix Biol.* 1999;18: 163-178.
36. Lovicu FJ, Kao WW, Overbeek PA. Ectopic gland induction by lens-specific expression of keratinocyte growth factor (FGF-7) in transgenic mice. *Mech Dev.* 1999;88:43-53.
37. Chikama T, Liu CY, Meij JT, et al. Excess FGF-7 in corneal epithelium causes corneal intraepithelial neoplasia in young mice and epithelium hyperplasia in adult mice. *Am J Pathol.* 2008;172:638-649.
38. Chanas SA, Collinson JM, Ramaesh T, et al. Effects of elevated Pax6 expression and genetic background on mouse eye development. *Invest Ophthalmol Vis Sci.* 2009;50:4045-4059.
39. Favor J, Bradley A, Conte N, et al. Analysis of Pax6 contiguous gene deletions in the mouse, Mus musculus, identifies regions distinct from Pax6 responsible for extreme small-eye and belly-spotting phenotypes. *Genetics.* 2009;182:1077-1088.
40. Shaham O, Smith AN, Robinson ML, et al. Pax6 is essential for lens fiber cell differentiation. *Development.* 2009;136:2567-2578.
41. Wolf LV, Yang Y, Wang J, et al. Identification of pax6-dependent gene regulatory networks in the mouse lens. *PLoS One.* 2009;4: e4159.
42. García-Villegas R, Escamilla J, Sánchez-Guzmán E, et al. Pax-6 is expressed early in the differentiation of a corneal epithelial model system. *J Cell Physiol.* 2009;220:348-356.

Role of the IL-6 Classic- and Trans-Signaling Pathways in Corneal Sterile Inflammation and Wound Healing

Nobuyuki Ebihara,[1] *Akira Matsuda,*[1] *Shinji Nakamura,*[2] *Hironori Matsuda,*[3] *and Akira Murakami*[1]

Purpose. To investigate the role of the IL-6 classic- and trans-signaling pathways in corneal sterile inflammation and wound healing.

Methods. To assess the production of inflammatory molecules by corneal fibroblasts treated with supernatant derived from necrotic corneal epithelial cells, the authors used an antibody array. Expressions of membrane IL-6 receptor (mIL-6R) and soluble IL-6R (SIL-6R) by fibroblasts and epithelial cells were detected with flow cytometry and RT-PCR. Expressions of signal transducer and activator of transcription 3 (STAT3), vascular endothelial growth factor (VEGF), and monocyte chemotactic protein-1 (MCP-1) by fibroblasts stimulated with IL-6 alone or IL-6/SIL-6R were determined by ELISA. The effect of IL-6 or IL-6/SIL-6R on epithelial cell migration was investigated in vitro by the scratch assay, whereas expressions of IL-6R and S100 A4 in the corneas of mice were detected by immunohistochemistry after incision of the corneal stroma.

Results. IL-1 derived from necrotic corneal epithelial cells induced the production of IL-6 by corneal fibroblasts. mIL-6R and SIL-6R mRNAs were expressed by both types of cells, although IL-6R protein at the cell surface was expressed only by epithelial cells. Expression of gp130 was detected in both types of cells. Activation of the IL-6 trans-signaling pathway induced the phosphorylation of STAT3, resulting in an increase of VEGF and MCP-1 production by corneal fibroblasts. Activation of the IL-6 classic-signaling pathway promoted the migration of corneal epithelial cells. IL-6R expression was also detected in activated fibroblasts and basal cells of the epithelium during the processes of wound healing in vivo.

Conclusions. The IL-6 classic- and trans-signaling pathways have an important role in corneal sterile inflammation and wound healing. (*Invest Ophthalmol Vis Sci.* 2011;52: 8549-8557) DOI:10.1167/iovs.11-7956

When cells die in vivo, a strong inflammatory response is initiated, including the rapid migration of neutrophils (followed by monocytes) into injured tissues. However, the mechanism that activates inflammation in response to cellular injury is not fully understood. There is evidence that necrotic cells release various endogenous "danger" molecules, such as high-mobility group box 1 protein (HMGB1), IL-1α, IL-33, heat shock protein 60 (HSP60), uric acid, S100 proteins, DNA, adenosine triphosphate, and β-defensin 2.[1-5] Among these danger signals, IL-1α has been investigated to assess its role in sterile inflammation of the cornea. Wilson et al.[6-8] reported that IL-1α/β are expressed by intact corneal epithelial cells and released into the corneal stroma after mechanical injury. Hong et al.[9] found that IL-1α has a crucial role in inflammatory cell infiltration into the cornea after epithelial scrape injury in rabbit. Recently, Stapleton et al.[10] examined the administration of a topical soluble IL-1 receptor antagonist on the infiltration of bone marrow-derived cells after corneal epithelial scrape injury in a mouse model, demonstrating that the IL-1 receptor antagonist dramatically suppressed the migration of CD11-b-positive monocytes into the corneal stroma. Therefore, IL-1α may be a master regulator of sterile inflammation, which occurs in response to injury of the cornea.[11] However, the mechanisms by which sterile corneal inflammation and wound healing are related to cell death have not been sufficiently investigated. Endogenous danger molecules released from necrotic corneal epithelial cells not only have a chemotactic effect on inflammatory cells, but also upregulate the production of chemokines by corneal fibroblasts.[8,9,12] In this study, we revealed that IL-1 derived from necrotic corneal epithelial cells induced the production of IL-6 and soluble IL-6 receptor (SIL-6R) by corneal fibroblasts.

IL-6 and SIL-6R are pleiotropic molecules that regulate inflammation and the immune response. Many researchers have found significantly increased concentrations of IL-6 and SIL-6R in the tear fluid of patients with Sjögren syndrome and vernal keratoconjunctivitis compared with the levels in healthy subjects.[13-17] Also, elevated levels of SIL-6R and IL-6 have been detected in the aqueous humor and vitreous fluid of patients with uveitis.[18] These findings suggest that IL-6 and SIL-6R may play an important role in several ocular inflammatory diseases. IL-6 is also known to be involved in wound healing, for example, IL-6-deficient mice show delayed cutaneous wound healing.[19-21] Nishida and colleagues[22-25] reported that IL-6 stimulates the migration of corneal epithelial cells both in vitro and in vivo. IL-6 is not involved in cell growth and differentiation, but makes a contribution to stem cell niche characteristics.[26,27]

Two different signaling pathways for IL-6 have been described. In the classic-signaling pathway, IL-6 binds to membrane-bound IL-6R (mIL-6R), leading to dimerization and activation of the signal-transducing protein glycoprotein 130 (gp130). On the other hand, in the trans-signaling pathway, IL-6 binds to SIL-6R and the IL-6/SIL-6R complex activates gp130. This trans-signaling pathway has some important biological effects. In particular, it enlarges the spectrum of targets for IL-6 because cells that do not express membrane-bound IL-6R can still be stimulated by the IL-6/SIL-6R complex. The level of ubiquitously expressed gp130 protein is believed to be relatively constant for all cells, whereas expression of IL-6R varies between different cell types. Through both the classic- and trans-signaling pathways, IL-6 activates signal transducer

From the Departments of [1]Ophthalmology and [3]Immunology, and the [2]Division of Biomedical Imaging Research, Juntendo University School of Medicine, Tokyo, Japan.

Submitted for publication May 29, 2011; revised September 6, 2011; accepted October 1, 2011.

Disclosure: **N. Ebihara**, None; **A. Matsuda**, None; **S. Nakamura**, None; **H. Matsuda**, None; **A. Murakami**, None

Corresponding author: Nobuyuki Ebihara, Department of Ophthalmology, Juntendo University School of Medicine, 3-1-3, Hongo, Bunkyo-ku, Tokyo 113-8431, Japan; ebihara@juntendo.ac.jp.

and activator of transcription 3 (STAT3) by phosphorylation of this molecule.[28-31]

Two mechanisms for generation of SIL-6R have been described in humans. First, SIL-6R can be formed via limited proteolysis of the membrane-bound receptor, a process called shedding. The second mechanism that can generate the soluble receptor is translation from alternatively spliced mRNA lacking the coding region for the transmembrane domain (DS-SIL-6R: differential SIL-6R splicing).[32,33] Recently, Sugaya et al.[17] revealed that corneal epithelial cells produced SIL-6R by shedding and alternatively spliced mRNA.

Although IL-6, SIL-6R, and STAT3 have been recognized as inflammatory mediators in the wound healing process, their role in corneal sterile inflammation and wound healing has not been adequately investigated. Therefore, we performed this study to assess the role of the IL-6 classic- and trans-signaling pathways in both sterile corneal inflammation and corneal wound healing.

Materials and Methods

Antibodies and Ligands

Mouse anti-human IL-6R and gp130 monoclonal antibodies (mAb) were purchased for flow cytometry (R&D Systems, Minneapolis, MN). Goat anti-mouse IL-6R polyclonal Ab (pAb) (R&D Systems) and rabbit anti-S100 A4 pAb (Thermo Fisher Scientific, Fremont, CA) were used in primary antibodies for immunohistochemistry. Other products used were as follows: FITC-conjugated donkey anti-goat IgG pAb (Santa Cruz Biotechnology, Santa Cruz, CA), biotinylated rabbit anti-mouse pAb (CosmoBio, Tokyo, Japan) (these antibodies were used in second antibodies for immunohistochemistry); recombinant human IL-1α, IL-6, and SIL-6R (PeproTech Inc., Rocky Hill, NJ); and recombinant human IL-1 receptor antagonist (ProSpec-TechnoGene Ltd., Rehovot Science Park, Rehovot, Israel).

Cell Culture

In experiments using human primary keratocytes and corneal epithelial cells (ScienCell Research Laboratories, Carlsbad, CA), keratocytes were primarily cultured in Dulbecco's modified Eagle's medium (DMEM) containing 10% fetal calf serum (FCS). The keratocytes showed transdifferentiation into corneal fibroblasts. Corneal epithelial cells (grown in FCS-free *Epimedium*; ScienCell Research Laboratories) were also used in primary culture.

Inducing Necrosis of Corneal Epithelial Cells

According to a previous report,[34] necrosis was induced by three cycles of freezing and thawing. Corneal epithelial cells cultured with serum-free DMEM were frozen (−80°C) for 20 minutes and thawed (37°C) for 20 minutes over three cycles. The supernatant obtained from necrotic corneal epithelial cells was used in this study. IL-6, SIL-6R, and MCP-2 were not detected in this supernatant by ELISA (data not shown).

Antibody Array

Culture supernatant obtained from corneal fibroblasts was analyzed with an antibody array (RayBio; Human Inflammation Antibody III kit; RayBiotech Inc., Norcross, CA) according to the manufacturer's instructions. Corneal fibroblasts were grown to subconfluence in DMEM containing 10% FCS, washed twice with PBS, and then incubated in serum-free DMEM for 24 hours with or without the supernatant of necrotic corneal epithelial cells (final concentration: 20%) or recombinant IL-1α (30 ng/mL). The culture supernatant was then harvested for antibody array analysis. To estimate the effect of IL-1 receptor antagonist, corneal fibroblasts were incubated in serum-free DMEM for 24 hours with the supernatant of necrotic corneal epithelial cells and IL-1 receptor antagonist (100 ng/mL), after which the culture supernatant was harvested for antibody array analysis.

Enzyme-Linked Immunosorbent Assay

To detect vascular endothelial growth factor (VEGF), monocyte chemotactic protein-1 (MCP-1), and phosphorylated STAT3 (Try705) in the supernatant of corneal fibroblasts, we used ELISA kits according to the manufacturer's instructions (Quantikine; R&D Systems). Corneal fibroblasts were grown to subconfluence and then incubated in serum-free DMEM for 24 hours with or without exposure to IL-6, SIL-6R, or IL-6/SIL-6R. The supernatant was then harvested for ELISA.

Preparation of RNA and RT-PCR

We examined the expression of two isoforms of IL-6R by using different primers for reverse transcription (RT)-PCR.[17] Total RNA was obtained from cultured corneal fibroblasts and epithelial cells (Nucleo Spin RNA II; Macherey-Nagel GmbH, Düren, Germany). RT-PCR was performed to examine the expression of mIL-6R and DS-SIL-6R, as described previously, using an mIL-6R sense primer (5′-cattgccattgttctgaggttc-3′), a DS-SIL-6R sense primer (5′-gcgacaagcctcccaggttc-3′), and a shared IL-6R antisense primer (5′-gtgccacccagccagctatc-3′). For mIL-6R, 40 cycles were performed with annealing at 60°C for 45 seconds. For DS-SIL-6R, 40 cycles were performed with annealing at 65°C for 45 seconds. PCR products were detected by electrophoresis on 1.5% agarose gel containing ethidium bromide, and bands were visualized under UV light.

Flow Cytometry

To detect the expression of IL-6R and gp130 protein by corneal fibroblasts and epithelial cells, we used flow cytometry (FACScan; BD Biosciences, San Jose, CA). After being washed with buffer, 10^6 cells were treated with Fc-block (BD Biosciences) for 15 minutes and then were incubated with mAbs targeting human IL-6R or gp130 or with isotype control mouse IgG (BD PharMingen, San Diego, CA) for 1 hour at room temperature. The cells were then washed twice with the buffer and incubated for 30 minutes with FITC-conjugated anti-mouse IgG. Finally, the cells were washed twice more with the buffer and analyzed. To gate out dead cells, staining with a kit containing propidium iodide was performed according to the manufacturer's instructions (BD Biosciences).

In Vitro Scratch Assay

Corneal epithelial cells were grown to confluence on six-well plates. A uniform wound was made in each plate using a 200-μL pipette tip, after which the plates were washed with PBS and incubated in Epimedium with or without IL-6, SIL-6R, or IL-6/SIL-6R. The wound area (immediately and 16 hours after creation) was observed and photographed. Experiments were done in duplicate, with three to five plates for each condition.

Animal Protocols

Female C57 BL6 mice (10 to 12 weeks old) were used in this experiment, and were handled according to the ARVO statement on the Use of Animals in Ophthalmic and Vision Research. The mice were given an intraperitoneal (IP) injection of ketamine (50 mg/kg) and xylazine (5 mg/kg) for deep anesthesia and a drop of 1% pro-paracaine for local anesthesia before creating stromal injury of the cornea. Stromal injury was then created by incision of the cornea with a blade while viewing the eye through an operating microscope. Twenty-four hours after corneal injury, the animals were euthanized with an overdose of pentobarbital (100 mg/kg, administered IP), after which the eyes were harvested and fixed in paraffin.

Immunohistochemistry

Paraffin specimens were cut into 4-μm sections, air dried, fixed in cold acetone for 10 minutes, and then washed in PBS. Next, the sections were blocked by incubation with 3% BSA, after which goat anti-mouse IL-6R pAb (1:50 dilution) was added and the slides were